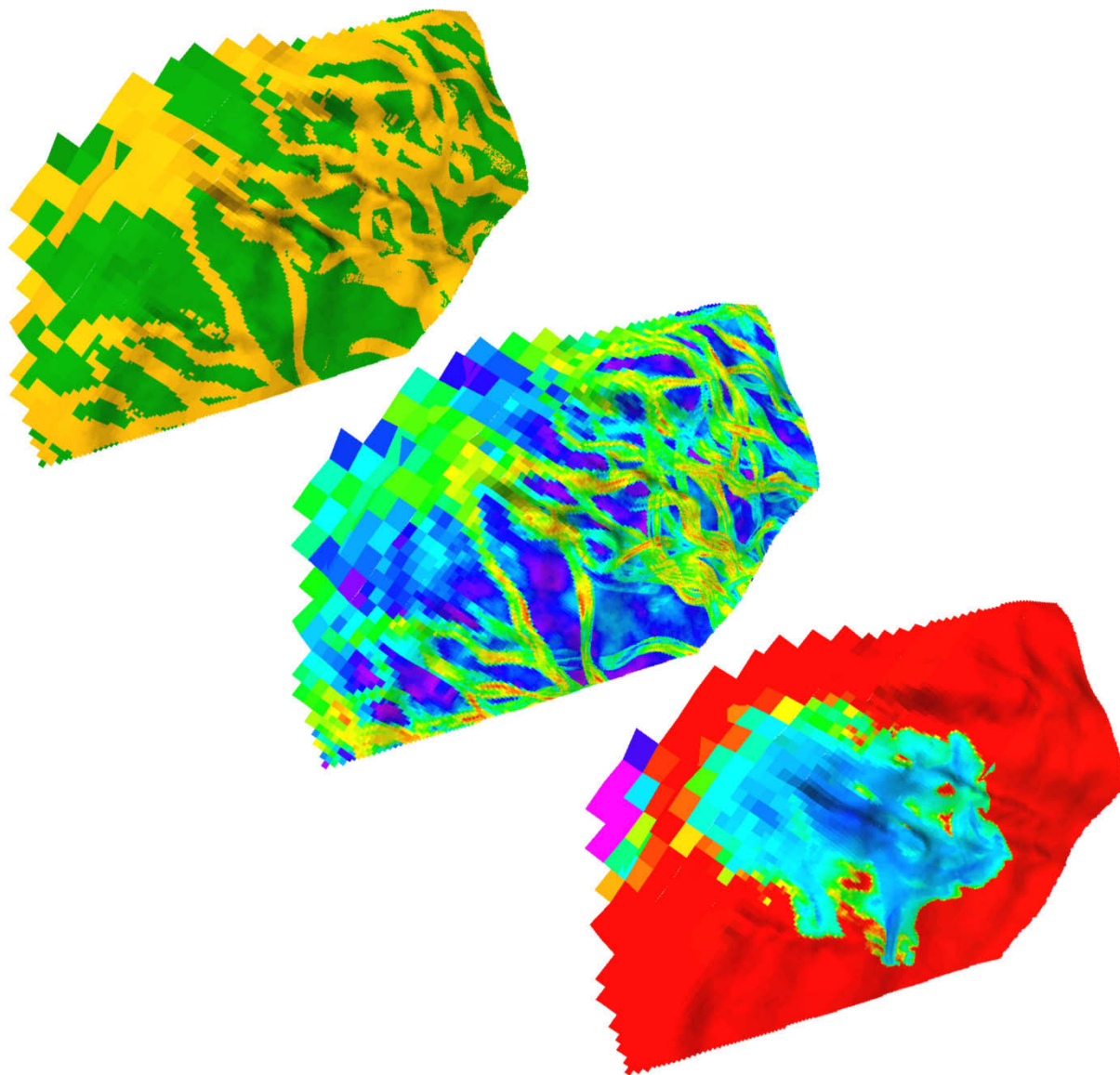


# Managing the Interdisciplinary Requirements of 3D Geological Models

---



Sarah Jane Riordan  
Australian School of Petroleum  
University of Adelaide  
March 2009

---

Thesis submitted in accordance with the requirements of the University of Adelaide  
for the degree of Doctor in Philosophy

---

## 3 DEPOSITIONAL ANALOGUES

### 3.1 Introduction

The interpretation of depositional environments from core or wireline logs is a critical phase in the construction of a 3D geological model. The interpretation of depositional facies provides the foundation of palaeogeographic maps for each unit interpreted. Once the interpretation of core and wireline has been carried out, the following issues need to be considered for the design of a 3D geological model:

- What are the dimensions of the sand bodies and heterogeneities associated with each facies?
- What modern or ancient analogues can be used to improve the interpretation of the facies distribution away from the wellbores?
- How much difference is there between the reservoir quality of different facies?
- How many facies need to be included in the model?
- How many flow zones are present, and how does this relate to the number of geological units interpreted?

This chapter summarizes the dimensions and properties commonly associated with each of the depositional environments interpreted in the Flounder Field. The values used in the construction of the facies models described in Chapter 4 are a combination of actual Flounder Field data and estimates derived from the analogue data described in this chapter.

When studying analogues of depositional systems care needs to be taken to separate the dimensions associated with modern systems from those associated with ancient systems. The geological record preserves an amalgamated (or eroded) portion of a system compared to modern surface expressions of the same environment.

Modern analogues are useful for providing an indication of the potential length and width of depositional features on a layer scale within a model. For example the width of modern

barriers may be an important indicator of how to model these systems. When building a 3D model of a barrier that transgresses across a field, an individual layer within the 3D geological model may be a close approximation of the visible part of a modern barrier island (Figure 3.1). In any given layer in a model, the geometry of sandbodies in a barrier facies should not try to reflect the amalgamated barrier that is preserved, but the actual likely width of the surface expression of the barrier or shoreface. The preserved amalgamated barrier will be represented by the total flow unit model.

Ancient analogues provide an indication of which facies are most likely to be preserved and significantly influence fluid flow through the reservoir. The thickness and width of amalgamated features such as channel belts and strandplains may be better estimated from ancient analogues where field (or regional) data does not provided sandbody boundaries.

The depositional environments interpreted in the Flounder Field are a strandplain, a barrier island and an incised valley filled with low sinuosity fluvial and estuarine deposits.

## **3.2 Strandplain Systems**

Strandplain systems are shore-parallel bodies of sand that form at the intersection of the land (coast) and the sea. Deposition of shoreface sediments occurs in the zone between the high tide mark and the storm-weather wave-base (Walker and Plint, 1992). Shorefaces can accrete to produce a strandplain (Curry et al., 1969). Strandplains are most likely to form on regressive, wave-dominated coastlines (Boyd et al., 1992).

The classic shallow marine model of a shallowing-upward vertical succession gives no indication of the lateral extent of the shoreface deposits (Howard and Reineck, 1981; Reynolds, 1999; Hampson and Storms, 2003). The thickness and lateral extent of shoreface deposits is the result of the interaction between sediment supply, shelf morphology, accommodation space and wave energy (Ainsworth et al., 2008; Howell et al., 2008). In strandplain systems the shoreface deposits are adjacent to the coast, whilst in barrier island systems a lagoon separates the shoreface from the coast.

### **3.2.1 Features of Strandplain Systems**

Modern shallow marine environments show a distinct ordering of sediments that is controlled by their position relative to the mean fair-weather wave base and mean storm-weather wave base (Walker, 1984). There are five main zones: backshore, foreshore, shoreface, offshore-transition and offshore (Elliott, 1986b; Walker and Plint, 1992) (Figure 3.2 & Figure 3.3). The overall vertical signature of most shallow marine deposits is one of coarsening and cleaning upward. The presence and thickness of these five elements is dependent upon a number of factors, which include: texture, sand supply, shelf morphology, base level, dominant weather conditions (storm, fair-weather or flood), and the ambient energy of the system (high, medium, low) (Clifton, 2006). Shoreface successions on high-energy coastlines are more likely to be thicker, and contain coarser sediments than those deposited on low-energy shorelines (Howard and Reineck, 1981). However thicker shoreface sediments do not have a corresponding increase in shoreface extent (Howard and Reineck, 1981).

#### ***3.2.1.1 Backshore***

The backshore is the area behind the foreshore. It is generally only inundated during storms, and is often separated from the foreshore by a shore-parallel ridge (berm) (Pryor, 1973; Elliott, 1986b). Bedding is most likely to consist of large scale cross-beds formed in aeolian dunes (Elliott, 1986b), but can also include parallel bedding of shore-parallel swale fill (Campbell, 1971). Bioturbation is likely to be sparse, and of low diversity (McEachern et al., 2005).

#### ***3.2.1.2 Foreshore***

The foreshore, or beach, is the intertidal area between the mean low tide line and the mean high tide line. It is dominated by the swash and backwash of breaking waves (Figure 3.2 & Figure 3.3). Bedding is most likely to be shore-parallel low-angle planar structures formed by wave activity in the swash zone (Walker and Plint, 1992). Bioturbation is absent due to the regular reworking of the sediments (Hampson and Storms, 2003).

### ***3.2.1.3 Shoreface***

The shoreface extends from the mean low tide mark to the mean fair weather wave base (Figure 3.2). There are numerous variations of the subdivisions within the shoreface zone. Clifton (2006) provides examples of the most common models. The subdivisions of the shoreface presented here are based on the model of Kamola and Van Wagoner (1995), which is defined by features identifiable in outcrop, rather than on modern shoreface morphology.

The upper shoreface is characterized by parallel and tabular cross-bedding (Kamola and Van Wagoner, 1995). Bioturbation, which is sparse due to the high energy regime, is dominated by vertical or u-shaped burrows (McEachern et al., 2005). The lower shoreface is characterized by a greater amount and diversity of bioturbation, swaley and hummocky cross-stratification (Kamola and Van Wagoner, 1995; Hampson and Storms, 2003) (Figure 3.3). The shoreface is dominated by coastal processes of onshore, longshore and offshore currents, and lacks features associated with delta fronts (e.g. mouth bars, distributary channels, hyperpycnites).

Onshore currents typically produce planar, low-angle cross-beds parallel to the beach face. Longshore currents produce cross-bedding oriented in the direction of the current. Seasonal influences can affect the direction of longshore drift. Offshore (rip) currents can cut shallow channels in shoreface sediments as they move water and sediment seaward past the breaker zone (Elliott, 1986b). Howard and Reineck (1981) showed that at any given time, bedding structures in modern shoreface sediments can reflect a variety of different sediment transport directions. However, Clifton (2006) argues that studies of ancient successions show that fair-weather structures are rarely preserved, and that it is storm-associated features such as longshore drift that dominate the geological record.

### ***3.2.1.4 Offshore - Transition***

The offshore-transition zone (also known as the inner shelf) extends from the fair-weather wave base to storm weather wave base (Figure 3.2). Suspension deposition of fine-grained sediment occurs during fair weather conditions, which is then reworked by organisms. During

storms, sediment is eroded from the upper beach face and redeposited offshore (Elliott, 1986b). Storm deposits are frequently reworked by fauna during fair-weather conditions. Where bioturbation has not occurred, hummocky cross-stratification (HCS) is commonly preserved. Individual beds of HCS are usually less than 1 m thick, and most commonly 0.1–0.5 m thick (Walker and Plint, 1992).

#### **3.2.1.5 *Offshore***

The offshore zone (also known as the outer shelf) is the region below storm wave base. The main sediment deposited is mudstone and siltstone, which is frequently intensely bioturbated.

### **3.2.2 Dimensions of Strandplain Deposits**

Strandplain systems often extend for hundreds of kilometres and can be tens of kilometres wide (Curry et al., 1969; Bhattacharya and Walker, 1991; Reynolds, 1999). Work by Reynolds (1999) shows that interpretation of a depositional systems tract can allow assumptions to be made about the potential dimensions of strandplain sandbodies (Figure 3.4). For example highstand shorefaces tend to be thicker and wider than transgressive shorefaces. Transgressive shorefaces have a mean width of 7.2 km, (min: 3.3 km, max 20 km, thickness:width ratio of 1:100), whilst sandbodies deposited in the highstand systems tract have a mean width of 16.4 km (min:16 km, max: 43 km, thickness:width of 1:1000) (Reynolds, 1999) (Figure 3.5). As strandplain deposits may be correlatable for hundreds of kilometres along depositional strike (Walker and Plint, 1992), it is the width, thickness, orientation and internal architecture of the flow units within the system that is most likely to influence fluid flow and hence the design of 3D geological models.

Where there is little shale in the system, distinguishing between a wave-dominated delta and a strandplain from wireline logs and limited core data can be problematic (Figure 3.3). In asymmetric wave-dominated deltas the upstream side of the delta mouth can look like a strandplain, whilst downstream of the river mouth fluvial deposits and lagoons can accumulate between beach ridges (Dominguez, 1996; Bhattacharya and Giosan, 2003)

(Figure 3.6). Shale has the potential to form on strandplains in the swales between the beach ridges. Clemmensen et al. (2001) describes peat layers approximately 0.8 m thick present in swales between beach ridges on the Skagen Spit in Denmark. Whilst Curray et al. (1969) note the seasonal flooding of the depressions between beach ridges of the Nayarit coast of Mexico they do not describe what, if any sediments are deposited as a result of this inundation.

There are numerous potential modern analogues for the lower Roundhead Member strandplain (for example Curray et al., 1969; Anthony, 1995; Tanner, 1995; Andrade et al., 2003). Modern analogues of paralic systems with well developed strandplains include the Nayarit coast on the west coast of Mexico, the deltas of the São Francisco, Doce, Jequitinhonha and the Paraíba do Sul rivers in Brazil. Individual strandplains of the deltas on the Brazil coast are all in the order of 50–80 km long—much larger than the Flounder Field. These deltas form an interlinked system up the Brazilian coast that stretches for approximately 1,800 km (Walker and Plint, 1992). The late Cretaceous coast of the Gippsland Basin could fit comfortably into either the Nayarit coast or the east coast of the Brazil (Figure 3.7). The Landsat image of the mouth of the Rio Doce, on the east coast of Brazil adjacent to the Atlantic Ocean shows all the elements interpreted in the Flounder Field (Figure 3.8). On the strandplain adjacent to the current channel, can be seen several palaeochannels of the river. These channels are adjacent to older strandplain deposits. The modern and palaeo- channels are relatively straight and narrow on the strandplain, and are approximately 200–1000 m wide. This is comparable to the interpreted width of the channel belts in the lower Roundhead Member.

### **3.3 Barrier-Island Systems**

Barrier islands are shore parallel, sandy, elongate islands or peninsulas that are separated from the mainland by lagoons or marshes (McCubbin, 1981). Barrier islands are most likely to form where there is a low gradient coastal shelf adjacent to a low gradient coastal plain, an

abundant sediment supply and moderate to low tidal ranges (less than 4 m) (Reinson, 1984). The majority of modern barriers are generated in a transgressive regime (Boyd et al., 1992).

There are four main hypotheses for the formation of barrier islands

- the segmentation of spits by tidal inlets (Figure 3.9),
- submergence of coastal beach ridges (Figure 3.10),
- the building up of submarine bars (Figure 3.11),
- the reworking of abandoned delta lobes during transgression (Figure 3.12).

Spit progradation is most likely to occur on coasts with high relief that are undergoing rapid transgression (Swift, 1975). Barriers that have formed via this method should have open marine sediments underlying the lagoon facies (Figure 3.9). Transgressive barrier islands formed by coastal submergence are most likely to occur on coasts with low relief (Swift, 1975). Rising sea level inundates the coast, flooding low areas between beach ridges (Figure 3.10). In this method of formation lagoon sediments should be underlain by coastal plain or sand ridges. Davis (1994) argues that this method of formation has few modern examples. The building of submarine bars that emerge during low tide and gradually build up to become permanently exposed was documented by Otvos (1981) on the Gulf Coast of Mexico along the Mississippi delta plain. Otvos (1981) used foraminiferal assemblages to interpret saline, open marine conditions underlying many of the barriers studied. Where brackish sediments do underlie barriers, an aggradational origin is still interpreted.

Transgressive barrier bar systems can be formed when abandoned delta lobes are eroded and replaced by barrier systems, which in turn are transgressed, leaving only submerged bars in a three-stage process (Penland et al., 1988) (Figure 3.12). Historical records in the Gulf of Mexico indicate the rapid formation and erosion of delta front barriers. The Isles Dernieres formed on a subsiding delta plain after 1853, and today are fast disappearing (Otvos and Giardino, 2004). This fragility suggests that Gulf Coast style recycled delta lobe barrier islands are not good analogues for barrier island deposits seen in the geological record as their preservation potential is poor. Stutz and Pilkey (2002) found the Mississippi model to be a relatively uncommon method of delta front barrier island formation.



There is continued debate about the most likely and/or common method of barrier island formation. Field and Duane (1976) concluded that although there are documented cases of barrier formation through shoal building, this process is insignificant in comparison to the other methods. However Davis (1994) notes that many barriers are formed via landward migration and upward accretion of sand, and states that this is possibly the most common method of barrier formation. Stutz and Pilkey (2002) found that approximately 30% of the world's barrier islands are associated with delta fronts, which are most likely to form through spit accretion. Hoyt (1967) found that numerous studies have shown that open marine sediments are not present landward of current barrier island systems—a situation that should occur if the barriers were formed via the aggradation of offshore bars. However Otvos (1981) and Otvos & Giardino (2004) found that barriers in the northern Gulf of Mexico are underlain by open marine sediments, and interpreted bar emergence as the mode of formation.

### **3.3.1 Features of Barrier Shorelines**

Modern barrier-shoreface systems show a mixture of depositional facies. The significant, common features of barrier-shoreface systems are: long (1–10's km), narrow (100's m) linear sand bodies, lagoons that separate the barrier island from the coastal plain, sub-tidal to sub-aerial beach-barrier dune complex, washover deposits, tidal channels and tidal deltas associated with lagoon openings (Reinson, 1992; Sixsmith et al., 2008) (Figure 3.13). As well as the shoreface facies (*section 3.2.1*), facies found in barrier-shoreface systems can include dunes, tidal channels & deltas, washover deposits and lagoons.

Barrier shorelines are geologically short-lived features (Bird, 1993). Stapor and Stone (2003) describe a Holocene barrier 20 km long, 3 km wide and 4 m thick, that radiometric dating indicates was deposited in less than 300 years. Similarly Penland et al. (1988) describe transgressive barriers that have formed after the abandonment of delta lobes of the Mississippi River less than 500 years ago. The process described by Penland et al. (1988) implies the destruction of the barrier islands as part of the cycle. Otvos and Giardino (2004) note that the Isles Dernieres, one of the islands that forms part of Penland et al's (1988) hypothesis has nearly disappeared a century after detachment from the delta lobe. Otvos

and Giardino (2004) document the preservation of barrier islands by burial under prograding delta marsh sediments.

In a regressive system the lagoon is likely to be overlain by coastal plain sediments, such as coals, as the barrier migrates seaward (Reinson, 1992). In a transgressive system the level of preservation of the barrier is dependant largely upon the rate of sea level rise (Davis and Clifton, 1987; Reinson, 1992). If relative sea level rises slowly then the barrier may be completely eroded as the shoreface moves landward. A wave ravinement surface, often seen in the geological record associated with a thin, coarse lag, will be created. The reworked barrier sands will be redeposited in washovers or inner-shelf storm sands deposits on the ravinement surface (Nummedal and Swift, 1987). The topography of the shoreline being eroded will also play a role in what, if any, sediments are preserved. Where the shoreline is deeply dissected, estuarine sediments may be preserved below the transgressive lag. Where this is not the case, the only evidence that a barrier existed may be the preservation of some lagoon deposits below the transgressive lag.

If relative sea level rises rapidly, the barrier may be drowned in place, resulting in the preservation of much of the barrier (Davis and Clifton, 1987). In this situation, the geological record may closely resemble the theoretical successions of barrier systems (Figure 3.13).

#### **3.3.1.1 Barrier**

The core of a barrier is made up of shoreface, foreshore, beach ridges and dune facies (Davies et al., 1971; Kraft and John, 1979; Reinson, 1984; Moslow and Tye, 1985; Elliott, 1986b; Reinson, 1992) (Figure 3.13). Modern barriers are frequently vegetated and aeolian sediments with root traces are sometimes preserved in the geologic record (for example Davies et al. (1971)). Preservation of foreshore and dune facies is unlikely transgressive barriers when the relative sea level rise is slow (Davis and Clifton, 1987).

Wave-dominated barrier shorefaces are generally long and thin (Figure 3.14), whilst tide-dominated barriers are generally shorter, thicker and often 'drumstick' shaped (Hubbard et al., 1979; Elliott, 1986b) (Figure 3.15).

### ***3.3.1.2 Tidal Inlets***

Tidal inlets are the conduit through the barrier that allows communication between the lagoon and the open sea (Figure 3.13). Tidal channel deposits are formed as the tidal channel migrates laterally and consist of an erosional base and associated coarse lag, overlain by bidirectional planar or trough cross-bedded sandstone that fines upward as the channel is filled in (Reinson, 1984). An idealised tidal channel has a sharp, erosive base, overlain by cross-bedded coarse sand and fining-upward to planar bedded sandstone if the abandoned channel is in a back barrier position (Figure 3.16). Where the channel is located on an active barrier the cross-bedded channel sands may be overlain by barrier dune deposits (Moslow and Tye, 1985).

The dominant processes on the shelf—wave vs. tide—will affect the geometry of the tidal inlet sand bodies. Hubbard et al (1979) describes three types of tidal inlets—wave-dominated, tide-dominated and transitional. Tide-dominated inlets are dominated by ebb flow, wave-dominated inlets are dominated by flood tides and in transitional inlets the ebb and flood flow is approximately equal and most sand is deposited in the channel itself rather than in the tidal deltas. Barrier islands in wave-dominated environments have few, if any permanent tidal inlets (Elliott, 1986b). Migrating channels produce tabular channel units that are significantly wider than the channel itself. In this situation, channel deposits can dominate in the geological record. Tidal inlets in wave-dominated settings are generally sand and shell-rich, fine to very coarse-grained cross-bedded deposits (Moslow and Tye, 1985) (Figure 3.16).

Where tidal processes dominate, tidal channels are likely to be ebb-dominated, deep and narrow (Hubbard et al., 1979; Elliott, 1986b). These channels laterally migrate slowly or remain fixed, producing lenticular, channel-shaped sandbodies that are isolated within the barrier sediments. Abandonment of the channel may result in the formation of a mud plug (Figure 3.16). Sediments deposited in tide-dominated tidal channels are generally fine grained, cross-bedded to burrowed mud and sand (Moslow and Tye, 1985).

---

### 3.3.1.3 *Tidal deltas*

Ebb- and flood-tidal deltas are formed at each end of the tidal channels (Figure 3.13). In tide-dominated inlets the ebb currents are extremely strong and will carry sediment a long way offshore (kilometres). Ebb tidal deltas in tide-dominated systems produce an arc-shaped ebb tidal delta (Hubbard et al., 1979; Reinson, 1992) (Figure 3.15). Sexton and Hayes (1996) showed that under some circumstances in a modern system, a large percentage (77%) of the reservoir quality sand deposited in barrier-shoreface systems can be associated with ebb tidal delta complexes—41% of which were deposited as channel fill sediments. The ebb tidal delta, on the seaward side of the barrier, is rarely preserved in the geological record as it is usually eroded by wave ravinement and longshore drift as the tidal channel migrates along the barrier (Figure 3.17).

Flood-tidal deltas are more likely to be preserved than ebb tidal deltas. Flood-tidal deltas are dominated by landward oriented sets of planar and trough cross-bedding, interbedded with ebb-directed cross-bedding towards the top of the succession (Elliott, 1986b). Flood tidal deltas may overlap as the tidal inlet migrates, creating a complex arrangement of bedforms. In a well developed tidal delta complex, there will be mutually exclusive ebb and flood channels. The ebb currents will flow through a deep central channel, whilst the flood currents will flow through shallower, marginal channels. Sediments deposited in the ebb tidal channel tend to be medium to fine-grained, clean sand, whilst sediments deposited in the smaller flood-tidal channels are commonly a mixture of sand and mud (Sexton and Hayes, 1996). A good modern example of a complex of flood tidal deltas can be seen in Moreton Bay Queensland (Lockhart, 2001) (Figure 3.17). In the Moreton Bay example the position of the channel has been stabilized by the vegetation of the barrier island.

### 3.3.1.4 *Washover Deposits*

Washover deposits are formed when wind-generated storm surges overtop and cut through the barrier, depositing sand in the lagoon (Reinson, 1984). Washovers form lobate or sheet deposits that are centimetres to a few metres thick and up to a few hundred metres wide, oriented normal to the barrier (Figure 3.18). Individual washovers can merge to form large

flats that cover large tracts of the barrier. Washovers are most commonly fine to medium-grained with bedding structures that consist dominantly of sub-horizontal planar beds and small to medium-scaled foreset strata where the washover enters the lagoon. Washovers can form a significant portion of the transgressive barrier sandbodies, and are one of the mechanisms by which barriers transgress landwards.

Barrier shorefaces can be an important indicator of sea-level rise and sediment supply (Sedgwick and Davis, 2003). Where sea-level rise and sediment supply are in equilibrium (e.g. slow SL rise and low sediment supply, or fast SL rise and high sediment supply) washover deposits will be the dominant facies as the barrier 'keeps up' with conditions. A rapid sea-level rise accompanied by low sediment supply will see the barrier 'give up' and deteriorate into swashover deposition. High sediment supply and low sea-level rise will result in progradation and a dominance of dune deposits, with fewer washover deposits.

#### ***3.3.1.5 Lagoons***

Lagoons are shore parallel bodies of water that are characterized by fluctuating salinity (Dickinson et al., 1972; Pemberton et al., 2001) and a variety of sediment sources (Reinson, 1984). Sediments deposited in lagoons include interbedded sand, silt, mud and organic material such as peat, salt marsh and mangroves (Hayden and Dolan, 1979; Reinson, 1984; Stutz and Pilkey, 2002). Sediment is deposited in lagoons via flood tidal channels, washovers and vegetation. Common features of lagoons include frequent bioturbation (diversity dependent upon salinity), oyster beds, bivalves preserved in articulated condition (Dickinson et al., 1972), and tidal flats showing evidence of emergence (Pemberton et al., 2001).

Lagoons in tide-dominated systems are often shallow and highly channelized whilst those in wave-dominated systems are more likely to be wide and open (Hubbard et al., 1979). The majority of deltaic lagoons, are fully vegetated by mangroves or salt marsh—primarily mangroves (Stutz and Pilkey, 2002).

Lagoon salinity is dependent upon climate, connectivity to the ocean and fluvial input. Lagoon salinity can vary from dominantly fresh water—where fluvial input is constant and

---

tidal inlets are transitory (for example the Gippsland Lakes prior to European intervention (Bird, 1993) to brackish where tidal channels are common and permanently open, to highly saline where fluvial input is limited, as is contact with the open marine environment.

### 3.3.2 Dimensions of Barrier-Shoreface System Deposits

Modern barrier shorefaces tend to be long narrow features. Everts (1987) describes a series of barrier islands on the mid-Atlantic coast USA ranging from 300–1000 m in width. Figure 3.19 shows measurements of a large number of barriers taken from Landsat images. They range in length from a few kilometres to tens of kilometres. The width of barriers is much more restricted—the majority of barriers measured were less than 1500 m wide, the widest measured (the Willapa barrier) was 3000 m. The surface dimensions of modern barriers are closely related to a variety of factors, which include tidal range, sediment supply, storm intensity and current intensity. Smith et al. (1999) attributes the unusual thickness of the Willapa barrier on the Washington coast to a combination of these factors. The Willapa barrier is 17–25 m thick, and is capped by dunes up to 18 m thick. In contrast, barriers described by Penland et al. (1988) on the Gulf Coast of the USA range in thickness from 1 to 13 m. Figure 3.20, taken from Riggs et al. (1992) highlights the difference between the amount of barrier visible at the surface compared to the overall width of the barrier deposits. A compilation of published widths of ancient barrier island deposits suggests that they are an order of magnitude wider than their modern counterparts (Figure 3.21). It should be noted that measurements of ancient deposits should be treated with some caution, as they may in fact include examples of shorefaces or wave-dominated deltas. Heward (1981) and more recently Clifton (2006) noted that these deposits can be difficult to distinguish in wireline log data and historically there may be an over-use of the barrier island model in the interpretation of ancient narrow sand bodies.

Ebb tidal deltas on abandoned lobes of the Mississippi delta (on a coast that has relatively low wave and tidal energy outside storm seasons) can extend offshore 2–6 km and be 6–8 km long (shore parallel) (Penland et al., 1988). In comparison, the ebb-tidal delta in Moreton Bay, Queensland, is approximately 8 km long, but is only 2–3 km wide (shore normal)

(Figure 3.17). Reynolds (1999) showed that in the geological record flood tidal-delta complexes tend to be twice as long as they are wide (Figure 3.22). They have an average length of 12.3 km and an average width of 6.2 km. There is a much poorer relationship between thickness and width or length—in general; they get thicker as they get larger.

Measurements of modern tidal channel widths indicates that modern tidal channels tend to be narrow—50% of measured channels less than 400 m wide, 80% less than 1000 m wide (Figure 3.23). It is recognised that measuring tidal channel widths on satellite images is risky as human interference in channel widths is not always easy to recognise at that scale, and no correlation with channel depth is possible. The width of modern tidal channels may provide a useful analogue for ancient deposits in tide-dominated systems where the tidal channels are relatively stable and filled by a mud plug upon abandonment. In wave-dominated systems the width of modern tidal channels is not likely to reflect the preserved tidal channel deposits, as the channel migrates along the barrier, leaving a sheet deposit behind (Hubbard et al., 1979; Moslow and Tye, 1985; Elliott, 1986b; Sixsmith et al., 2008). Sixsmith et al. (2008) measured multistory tidal-channel fill complexes that were 500–2700 m long (depositional strike), 500–2500 m wide (depositional dip) and 6–14 m thick.

## **3.4 Incised Valley Fill**

The model being used for the fluvial filled incised valley is that of a wave-dominated estuary as described by Dalrymple et al. (1994) and Zaitlin et al. (1994). The progression from fluvial sediments at the base of the channel through to estuarine sands, offshore shale capped by a transgressive bar is typical of the seaward portion of an incised valley system (Figure 2.27).

### **3.4.1 Features of Low Sinuosity Fluvial**

Bridge (2006) concluded that it is not possible to identify channel characteristics (braided vs. non-braided) from vertical lithofacies successions (wireline logs). He argues that these distinctions can only be made by examining the accretion patterns of channel bars in large scale inclined strata in cross section. However, in the absence of not only outcrop but also

---

numerous, distinct bedding planes in the core, the wireline signature (gamma and sonic logs) is the main diagnostic tool used in this project.

In fluvial deposition, the level of heterogeneity is strongly dependent upon the relationship between accommodation and sediment volume. Sand-bodies deposited in low-sinuosity channels have distinctly different morphologies from those formed in meandering channel systems (Davies et al., 1993) (Figure 3.24). High sinuosity systems deposit sediment by lateral accretion, commonly in heterolithic point bars. Channels fill with silt and mud once the sediment supply is removed as a result of channel abandonment. This produces sand-bodies with the classic 'fining-upward' log signature (Walker and Cant, 1984). Low sinuosity meandering channel systems deposit sediment by vertical accretion of in-channel bars that cover most of the channel floor (Figure 3.25). This produces a stacked succession that exhibits no consistent vertical change in grain size or sedimentary structures (Davies et al., 1993). Mid-channel bars are made up of complex depositional patterns (Best et al., 2003; Lunt et al., 2004) (Figure 3.26). Sedimentary structures are dominated by horizontal to very low angle planar and trough cross-bedding. Thin layers of clay can be deposited during channel abandonment, but these are generally reworked into clasts by subsequent channels and are frequently of limited aerial extent (Davies et al., 1993).

### 3.4.2 Features of Estuaries

Dalrymple et al. (1992) defined an estuary as "*the seaward portion of a drowned valley system which receives sediment from both fluvial and marine sources and which contains facies influenced by tide, wave and fluvial processes. The estuary is considered to extend from the landward limit of tidal facies at its head to the seaward limit of coastal facies at its mouth*". Facies models of estuaries generally divide them into two types—tide-dominated and wave-dominated (Dalrymple et al., 1992; Reinson, 1992; Boyd et al., 2006) (Figure 3.27). The estuary sediments identified in the upper Roundhead Member are interpreted as having been deposited in a wave-dominated estuary. The principal elements of this system are the bayhead delta, mudflats, the central basin mudstones and the barrier island–tidal delta complex. Wave-dominated estuaries differ from lagoons associated with barrier island



in that lagoons have no or minor fluvial input and no strong association with a drowned river valley (Boyd et al., 1992; Boyd et al., 2006) (Figure 3.28).

#### ***3.4.2.1 Central Basin***

The central basin is an area of generally low energy where the fluvial outflow meets the marine inflow, resulting in brackish and often variable salinity conditions (Dalrymple et al., 1992) (Figure 3.29). Features of this environment include flaser bedding, double mud drapes and laminated mud and sandstone (Roy et al., 1980; Dalrymple et al., 1992; Nichol et al., 1997; Peijs-van Hilten et al., 1998; Boyd et al., 2006). The central basin deposits may also include peat, coal, mudflats and oyster beds (Washington et al., 1994; Boyd et al., 2006). The central basin deposits often show high levels of bioturbation but a limited diversity of species due to the brackish conditions (McEachern et al., 2007).

#### ***3.4.2.2 Bayhead Delta***

The shape of bayhead deltas is the result of interaction between the morphology of the estuary, the sediment load (gravel or fines) and tidal influence. A broad lagoon shaped estuary is likely to produce a birdfoot style delta, whilst a narrow estuary is more likely to produce a funnel shaped deposit (Dalrymple et al., 1992). A narrow estuary with sand rich input coupled with high tidal range is likely to produce funnel shaped sand bars, as is seen in the Bay of Fundy (Dalrymple and Zaitlin, 1994), whilst low tides and a higher mud content is more likely to produce a birdfoot style, fluvial dominated delta. Delta shape also changes as the delta progrades and fills the estuary (Roy et al., 1980) (Figure 3.30).

### **3.4.3 Dimensions of Incised Valley Fill Deposits**

#### ***3.4.3.1 Low Sinuosity Fluvial Channels***

The only data available for the Flounder Field are core and wireline logs. Methods such as the direct estimation of channel dimensions from 3D seismic are not applicable, due to the poor seismic resolution at this depth and will not be discussed. Other, potentially useful methods for determining width to thickness relationships discussed in the literature include:

- Identifying single story sandstone bodies in core or wireline logs and plotting channel depths on charts of width vs. thickness compiled from outcrop data (studies include: Fielding and Crane, 1987; Robinson and McCabe, 1997; Reynolds, 1999; Gibling, 2006). The most recent publication of this methodology is Gibling (2006).
- Estimating channel depth from the thickness of channel bars and strata associated with dunes to channel width using empirical equations or outcrop data (Bridge and Mackey, 1993; Bridge and Tye, 2000; Bridge, 2006).

All methods require the identification of bankfull depth of individual channels (Leeder, 1973; Collinson, 1978; Lorenz, 1985; Fielding and Crane, 1987; Bridge and Mackey, 1993; Robinson and McCabe, 1997; Bridge and Tye, 2000; Bridge, 2006; Gibling, 2006). The channel depth can then be related to channel belt width. Fielding and Crane (1987) proposed that channel depths be estimated in wireline logs by blocking well logs to remove any sandbody less than 2 m thick. This removed non-channel deposits from the calculation. These thicknesses could then be plotted on a width/thickness chart to establish channel belt thicknesses for each sandbody in an area of interest (Figure 2.39). The cross sectional area of each body could then be calculated and a statistical summary of the sand bodies in a field could then be estimated, and the dimensions of potential future penetrations be predicted.

Bridge (1985), Bridge et al. (1986), Bridge (1993), Bridge and Mackey (1993), Bridge and Tye (2000) and Bridge (2006) argue that methods that estimate channel depths by identifying individual channels in core or wireline logs are incorrect. This is due to the difficulties associated with distinguishing between channel bodies and overbank deposits, and with identifying complete individual channels in environments where younger channels are likely to have intersected and eroded older ones (Figure 3.31). Bridge and Tye (2000) propose that channel depth is better estimated by identifying dune height and the thickness of large scale cross-strata, as there is a known relationship between dune height and water depth.

The width of channel belts is also related to the ratio of channel bodies to overbank deposits (Bridge and Mackey, 1993). If the amount of channel bodies exceeds 75% of the total volume then the channel belts will all be connected and sandstone body may extend across

the entire floodplain. If the amount of channel bodies is between 40–75%, the channel belt thicknesses and channel belt widths increase with increasing channel content. Where there is less than 40% channel volume, channel belts will not be connected, and the sandstone body widths and thicknesses will approximate those of the individual channel. In the case of the Flounder Field, the sand content of the RU.1 unit is in the order of 80–90%. As can be seen from the log signature plot, the sandbody covers the entire field (Figure 2.42). Although it is very difficult to identify individual channels from the wireline logs, an attempt has been taken to subdivide the blocky sandstone packages into smaller possible channel units. The numbers that result from this exercise (min thickness: 3 m, max: 11 m, mean: 6 m) provide a range of values for channel belt width (min channel belt width: 90 m, max: 3,000 m, mean: 300 m,) that indicate that it is likely that the lower RU.1 unit consisted of more than one channel belt covering the Flounder Field (6x12 km area) (Figure 3.32). The width:thickness ratio of the total incised valley fill has also been compared to the data compiled by Gibling (2006). The width:thickness ratio of the incised valley shown on the palaeogeographic maps for the upper Roundhead units (Figure 2.43) is similar to ancient analogues compiled by Gibling (2006) (Figure 3.33). This suggests that the incised valley in the Flounder Field could be up to 20 km wide and remain within the width:thickness envelope for this style of incised valley fill.

#### ***3.4.3.2 Estuarine Deposits***

The dimensions of estuarine deposits found in an incised valley are restricted to the size of the incised valley. The dimensions of bayhead delta deposits can be difficult to establish. Plint and Wadsworth (2003) showed that the distribution of coarsening-upward bayhead delta deposits can be randomly scattered amongst channel fill deposits.

### **3.5 Porosity and Permeability Distribution**

Porosity is the ratio of pore volume to bulk volume, whilst effective porosity is a measure of interconnected pore spaces. Porosity is related to sorting and grain shape. Well sorted materials generally have higher porosity than poorly sorted ones, and angular sands are

---

usually more porous than well rounded ones (McLane, 1995). In theory, porosity is independent of grain size, but in practice finer sands are often more porous than coarser ones—apparently due to a tendency of fine particles to be less rounded (McLane, 1995).

Permeability is the ability of a medium to transmit fluid (Pettijohn et al., 1987). Permeability is measured by forcing a fluid to flow through a rock at a specific rate and pressure.

Permeability is calculated using Darcy's law:  $Q = \frac{k}{\mu} A \frac{\Delta P}{L}$ , where  $Q$  is the flow rate,  $k$  is the permeability,  $\mu$  is the viscosity,  $A$  is the cross-sectional area,  $\Delta P$  is the change in pressure across the sample and  $L$  is the length of the sample. In a rock sample, permeability will be different depending on the orientation of the sample relative to the rock fabric. This is known as directional permeability. This occurs because permeability is related to pore volume, grain size, orientation, sorting and ductile grain content (Mast and Potter, 1963; Masch and Denny, 1966; Dodge et al., 1971; McLane, 1995; Dutton and Willis, 1998). Bedding features such as cross-beds and shale drapes contain enough variability in grain size for directional permeability to be apparent at a bedding scale (Greenkorn et al., 1964; Weber, 1980; Lasseter et al., 1986; Lewis, 1988; Hurst and Rossvoll, 1991.; Pickup et al., 1994b).

Different depositional environments will create rocks with different characteristics, which will in turn affect permeability. Dodge et al. (1971) showed that alignment and frequency of cross-bedding laminae will affect permeability and set up preferred directions of maximum permeability. There will be maximum permeability in beds with a low angle of dip, while highly dipping beds will impede flow, as there are more interfaces to cross. As cross-bedded sediments have maximum horizontal permeability along depositional dip, the direction of maximum permeability in fluvial environments approximates the orientation of the fluvial channel. Pickup and Hern (2002) showed that the ratio of low to high permeability laminae will influence overall effective permeability. Where low permeability laminae are thin relative to high permeability laminae, their influence is less than where the laminae are of similar thickness. Ringrose et al. (1999) found that the importance of small-scale features is related to the complexity of the reservoir. In apparently simple reservoirs, such as a shoreface deposit, small-scale features will usually have primary importance. In complex reservoirs,

such as stacked sands deposited in a meandering fluvial environment, small-scale features will usually be of secondary importance as connectivity between sandbodies dominates flow patterns. Hurst and Rossvoll (1991) showed that permeability anisotropy in cross-bedded sandstones can be identified in both core plug and minipermeameter measurements. They also demonstrated significant differences in permeability measurements between various techniques, with the permeability contrast being lessened as the scale of measurement increased.

### **3.5.1 Permeability of Barrier Island Systems**

The permeability distribution in barrier island systems follows the orientation of the facies elements and the grain size distribution. Permeability is generally best in the shoreface facies of barrier islands (Galloway and Cheng, 1985; Honarpour et al., 1988; Hamilton, 1995). Permeability contours in barrier cores follow the strike of the barrier, with the greatest permeability occurring at the top of the sandbody (Galloway and Cheng, 1985; Sharma et al., 1990). The permeability contours in tidal inlets are dip oriented, with the best permeability occurring at the base of the channel. In back barrier facies the distribution of permeability is erratic and heterogeneous (Galloway and Cheng, 1985).

Stalkup and Ebanks (1986) found that mean permeability trends in the barrier island–tidal delta facies in the Ferron Sandstone can remain constant laterally for 60–150 m before a statistically different mean permeability is encountered. Permeability contrasts can also be up to three fold over this distance, but 1.5 to 2 is more usual.

### **3.5.2 Permeability of Shoreface Systems**

Shoreface deposits are noted for being continuous along strike for tens to hundreds of kilometres, and down dip for up to tens of kilometres. Permeability trends within shoreface sandstones reflect these depositional trends. Pryor (1973) found shore parallel trends on modern beach sections. There were differences normal to the shoreline associated with differences in grain size and packing between the beach face, crests and berms. The

direction of maximum permeability was oriented perpendicular to the shoreface in the beachface, landward in the berm area behind the beach crest, and parallel with the shoreface in the back-berm areas. Dodge et al. (1971) also noted a variety of orientations for maximum horizontal permeability in shoreface deposits. Pryor (1973) measured three beach sections approximately 600 m long and all showed relatively uniform shore-parallel permeability values.

Permeability in ancient cross-bedded shoreface sands can change by an order of magnitude over a very short (0.3 m) horizontal distance due to variations in grain size and sorting related to depositional structure (Castle et al., 2004). Permeability of bioturbated lower shoreface deposits can be significantly less than the upper shoreface. Castle et al. (2004) found an order of magnitude difference in the geometric mean permeabilities of lower and upper shoreface sediments. While bioturbation can significantly lower horizontal permeability in sandstone beds by disrupting bedding planes, vertical burrows through shale layers have the potential to enhance vertical permeability (Weber, 1980; Castle et al., 2004; Gingras et al., 2005).

In ancient deposits, visually obvious changes in grain size are topsets and clinoforms related to shoreface progradation. Clinoform boundaries are frequently draped with shale, and thus are potential flow boundaries (Wehr and Brasher, 1996). Shale draped clinoforms are more common in fluvial dominated deltaic systems than in wave-dominated shoreface systems such as the lower Roundhead Member (Howell et al., 2008). Clinoforms follow the trajectory of the shoreline, thus potentially creating shore parallel permeability baffles and barriers (Hampson, 2000). However Hampson (2000) notes that intra-parasequence clinoforms may only extend along depositional strike for 500–1500 m, and down depositional dip for 100–6000 m, and as such may not form regional field-wide permeability baffles or barriers. In the shallow marine environment, parasequence boundaries can form regional permeability barriers as they are marked by shale layers associated with the rise in base level (Kamola and Van Wagoner, 1995). However permeability barriers caused by parasequence boundaries or changes in shoreface profile can be breached by fluvial incision (Castle and Miller, 2000).

### **3.5.3 Permeability of Fluvial Systems**

The permeability of fluvial sandstones is strongly influenced by stratification styles. Planar-bedded and cross-bedded sandstones are likely to have much higher permeability than rippled sandstones (Jones et al., 1987; Davies et al., 1993; Hartkamp-Bakker and Donselaar, 1993; Doyle and Sweet, 1995; Liu et al., 1996). Hartkamp-Bakker and Donselaar (1993) measured permeability of point bars in outcrop and found distinct differences in permeability between the poorly sorted bottomsets (low perm) and the moderately to well-sorted foresets.

Maximum horizontal permeability tends to follow the depositional axis (Dodge et al., 1971; Pryor, 1973; Jones et al., 1987). Pryor (1973) measured permeability in modern river bars and found that permeability decreases downstream and bankward as grain size decreased.

Dreyer et al. (1990) showed that in low sinuosity, thin channels, permeability is greatest in the centre of the channel and low near the edges. They note a correlation length for permeability variograms (in the direction of palaeoflow) of 2–3 m only. Permeability trends appear to form lenses in the direction of the palaeoflow. The paradigm that permeability decreases upward in the channel was not born out in this study—with high permeability zones near the tops of active channels in the infill stage.

Vertical permeability is often poor in fluvial sandbodies due to the presence of shale drapes. However, it can be improved by dewatering structures which disrupt shale drapes (Jones et al., 1987).

## **3.6 Flow Unit Boundaries**

Flow units are regions within the total rock volume within which the geological and petrophysical properties that affect fluid flow are internally consistent and predictably different from properties of other rock volumes (Ebanks, 1987). In all the depositional systems discussed, potential flow unit boundaries (features that cause a change in flow conditions) are likely to be related to components of the systems tracts.

In the shallow marine environment sequence and parasequence boundaries, marine flooding surfaces and transgressive surfaces of erosion are regional features which have the potential to bring significantly different facies into contact (Plint, 1988; Van Wagoner et al., 1988; Dalrymple et al., 1992; Zaitlin et al., 1994; Kamola and Van Wagoner, 1995; Emery and Myers, 1996). Marine flooding surfaces that form parasequence boundaries are widespread features, and as such have the potential to act as vertical flow barriers. All these surfaces may indicate points at which shoreface widths, stacking patterns and depositional environments have the potential to change significantly. Kjønsvik et al. (1994) showed that the offset of parasequences and interfingering of facies has a significant impact on fluid flow. Whilst Wehr and Brasher (1996), Ainsworth et al. (1999) Cook et al. (1999) and Larue and Legarre (2004) show the influence of chronostratigraphic correlations and clinof orm boundaries on the results of reservoir simulation. Thus care needs to be taken to identify individual parasequences so that the juxtaposition of facies between parasequences can be understood.

In the fluvial environment changes in systems tract can be accompanied by changes in style of fluvial deposition and changes in net sand content and channel connectivity (Shanley and McCabe, 1991; Posamentier and Allen, 1999) (Figure 3.34). Although the sequence boundaries and flooding surfaces may be more subtle, they have the potential to form flow unit boundaries or mark a point at which stacking patterns change significantly, and therefore need to be modelled separately. Lowstand fluvial systems are generally sand-rich, whilst transgressive and highstand systems are more likely to have lower net sand ratios, less channel connectivity and more internal baffle and barriers due to the presence of overbank fines and coals (Shanley and McCabe, 1991; Emery and Myers, 1996; Posamentier and Allen, 1999).

The chronostratigraphic interpretation of the Flounder Field can be used to define potential flow units within the reservoir (Figure 2.49). The boundaries between the systems tracts are defined by incision or flooding surfaces and represent points at which different depositional facies may be juxtaposed.



## **3.7 Discussion – Depositional Environments**

### **3.7.1 Uncertainty**

The ways in which an interpretation of depositional environments influences the building of 3D models is summarized in Figure 3.35. When building 3D geological models using an interpretation based on core and wireline data the most important question is often “what are the dimensions of the depositional elements being modelled?” As shown, there are papers that bring together a wide variety of studies in order to generate width/length/thickness statistics (papers used in this study are Fielding and Crane, 1987; Reynolds, 1999; Gibling, 2006). A common feature of these papers is that they include width/thickness plots that show a wide spread of data points (an order of magnitude spread is not uncommon). Although the well data may narrow down the choice of values, this highlights an area of major uncertainty when using analogues. Not only is the interpretation of depositional environment important, but so is the choice of analogue or statistical measurement that is used. In this project, areas of uncertainty relating to depositional system are as follows:

- The lower Roundhead Member may be a strandplain or part of wave-dominated delta. The differences to the way a model is built would be:
  - Shape of sandbody—strandplain long, linear feature whilst a wave-dominated delta may have triangular wedge shape (Curry et al., 1969; Dominguez et al., 1987; Anthony, 1995; Dominguez, 1996; Andrade et al., 2003),
  - Orientation of channels (perpendicular to coast on a strandplain, or angled, originating from a single source on a delta) (Howell et al., 2008). Although this may not result in much difference in channel distribution for a small field such as Flounder, on large fields that are more likely to encapsulate a greater portion of a delta this could be significant.
  - Shale distribution—shales deposited on a strandplain are likely to have different distribution, thickness and length from those deposited on a delta

---

(Zeito, 1965; Weber, 1980; Bhattacharya and Giosan, 2003). Furthermore, shale distribution on a delta is indicative of the relative influences of wave and river discharge (Howell et al., 2008).

- The interpretation of a delta or strandplain may have implications for the vertical permeability of the reservoir and ultimate performance of a dynamic model (Figure 3.36).
- The width of a strandplain is influenced by the systems tract in which it is deposited (Reynolds, 1999). Thus, the interpretation of overall width of the deposit, (which exceeds the well data) is dependent upon the position of the shoreface in the sea-level cycle, (Figure 3.4)
- The upper Roundhead Member fluvial sandstone is interpreted to have been deposited in a low sinuosity fluvial setting, but could be a meandering river system with very low accommodation space. The differences to the way a model is built would be:
  - Shape of bedding planes, and intra body surfaces. These may have a very strong influence on fluid flow, but are below the scale of the models built in this project. The applicability of models that capture fine bedding detail to field scale datasets is a subject in need of future discussion. Future computing power will allow for the building of extremely detailed models, but they will not necessarily provide any greater accuracy of modelling in inter-well areas than coarser models.

### 3.7.2 Permeability

Models of depositional environments are the precursor to the construction of permeability models for reservoir simulation. Permeability is influenced by rock characteristics at many scales. Lasseter et al. (1986) show that although heterogeneities at all scales can influence reservoir behaviour, it is the large scale features, such as faults and facies changes, that are most likely exert significant control on hydrocarbon recovery and bypass. Mijnsen et al. (1990) argue that although many depositional elements within deltaic deposits have

characteristic, and different, shapes, a number of them have very similar internal characteristics, and thus flow properties. By classifying depositional elements into eight elementary flow unit types, they were able to show that horizontal permeability anisotropies are only significant in simulation studies for depositional facies with abundant inclined shales.

The frequency, distribution and size of shale layers have a significant impact on vertical and horizontal permeability in reservoirs (Zeito, 1965; Richardson et al., 1978; Weber, 1980; Haldorsen and Lake, 1984; Begg and King, 1985; Weber and van Guens, 1990). Weber (1980) and Haldorsen and Lake (1984) showed that depositional environments can be used a predictor for shale length and frequency, which can then be used to generate statistical models of shale distribution in 3D models (Figure 3.36).

Although outcrop data is an excellent source of permeability trends and relationships, there are several factors that need to be kept in mind when applying it to another reservoir. In particular, outcrops have a very different burial history to their subsurface counterparts. This will influence diagenetic patterns as well as overall permeability (Dutton and Willis, 1998). Dutton and Willis (1998) show a change from bimodal permeability distribution to unimodal distribution between rocks of the same formation in outcrop (unimodal) and subsurface (bimodal). Such differences are even more distinct between measurements of modern sediments and buried rocks. Also, weathered outcrop permeability can be orders of magnitude lower than unweathered outcrop rock due to surface diagenesis (Dutton and Willis, 1998).

Depositional fabric will also influence post depositional features such as compaction and diagenesis (Dutton and Willis, 1998; Salem et al., 2005). Salem et al. (2005) found differences in diagenesis in a incised valley system between LST fluvial sediments and TST estuarine deposits that they related to the differences in grainsize, lithology and the formation fluids during early burial.

In the Flounder Field four depositional environments were interpreted: barrier island, strandplain, lowstand incised valley fill low sinuosity fluvial channels and estuarine. These depositional environments have different sand and shale distributions, which will influence

the vertical and horizontal permeability of the units interpreted (Haldorsen and Lake, 1984; Begg and King, 1985; Lasseter et al., 1986). The modern and ancient analogues cited in section 3.5 indicate that these environments also have potentially different permeability patterns within their sandbodies. As a result they should be regarded as separate flow units for modelling purposes (Ebanks, 1987).

### **3.8 Conclusions – Depositional Analogues**

The availability of satellite imagery on the internet has made finding high quality images of modern depositional systems relatively easy. Satellite images give an excellent overview of the dimensions of large scale features in these environments, which is a good starting point for designing a 3D facies model (Figure 3.1). However, modern analogues need to be chosen with care. The best looking, most easily measurable images are usually those of very large systems. Thus, studies of width:thickness ratios of ancient deposits need to be used as a reality check for the dimensions of any given deposit. In order to do this, as much data as possible should be gathered to narrow down the spread of possible values.

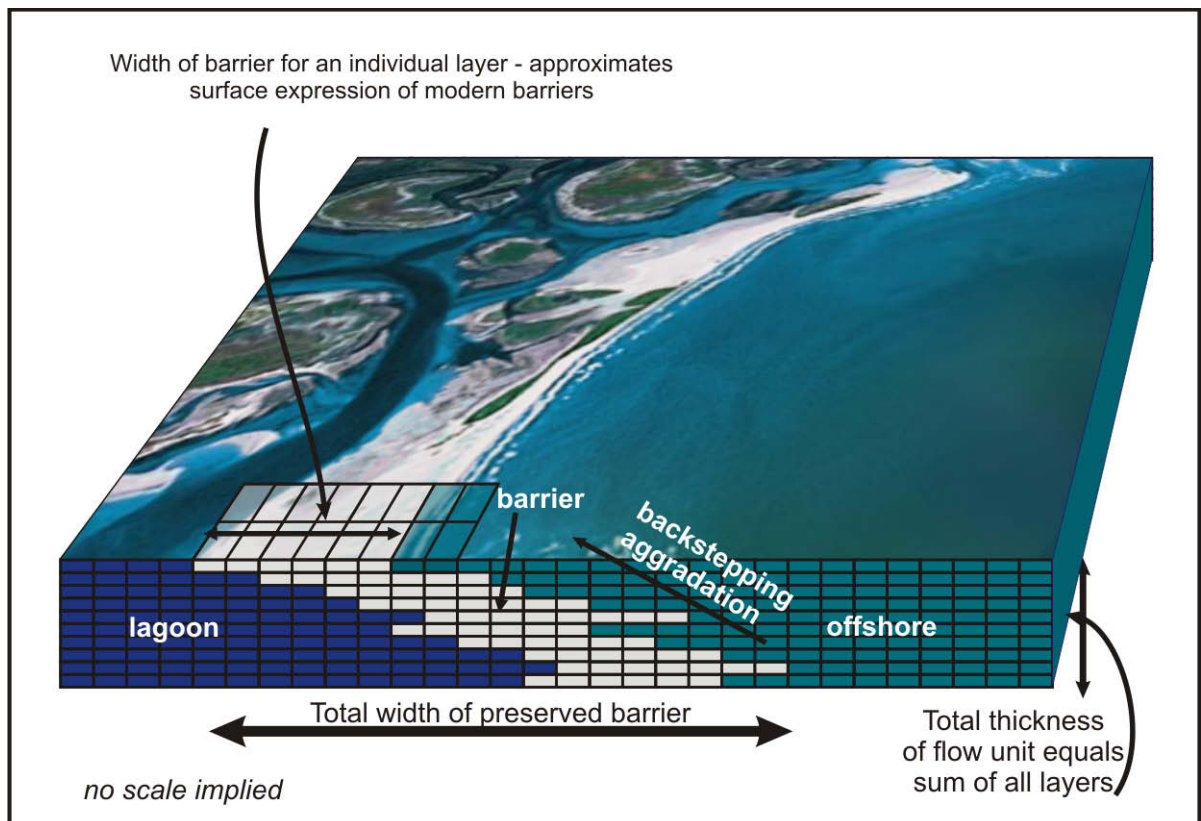
Correct interpretation of the scale of fluvial deposits is difficult from wireline data alone. Where there is the uncertainty in the interpretation of depositional environment, the differences this could cause in the way a model is constructed should be documented and included in a summary of the uncertainties associated with a geological model. Similarly, in a paralic system distinguishing between a barrier island system and a strandplain is essential as the two environments have very different dimensions even though some depositional facies are common to both. During the modelling process, production data may indicate that one interpretation and its associated parameters may be more applicable than another.

As computers get more powerful, the amount of cells that can be put in a model will continue to increase. As this occurs, it will be necessary to consider how to model the internal structures of sandbodies. This will place an even greater importance upon understanding the differences between possible depositional environments.



### **3.9 Figures – Depositional Analogues**





**Figure 3.1. Schematic showing how the width of modern barrier islands or strandplains can be used as an analogue for the modelling of ancient systems.** The amalgamated width seen when creating palaeofacies maps from genetic units is honoured by the overall width and thickness of the flow unit, while the modern width is used as a guide for the width of the facies for an individual layer. From (Riordan et al., 2008). Photo from Google Earth.



NOTE:  
This figure is included on page 122 of the print copy of  
the thesis held in the University of Adelaide Library.

*Figure 3.2. Shoreface elements.* Modified from Walker and Plint (1992).

NOTE:

This figure is included on page 123 of the print copy of the thesis held in the University of Adelaide Library.

**Figure 3.3. Idealized vertical shoreface profile.** From Clifton (2006), who states that this “standard model” is most applicable to a storm-dominated, moderate- to low-energy setting with a moderate gradient in which fine sand is in somewhat limited supply and the base level was static. This model is very similar to the succession seen in a wave-dominated deltas (Bhattacharya and Giosan, 2003).

NOTE:

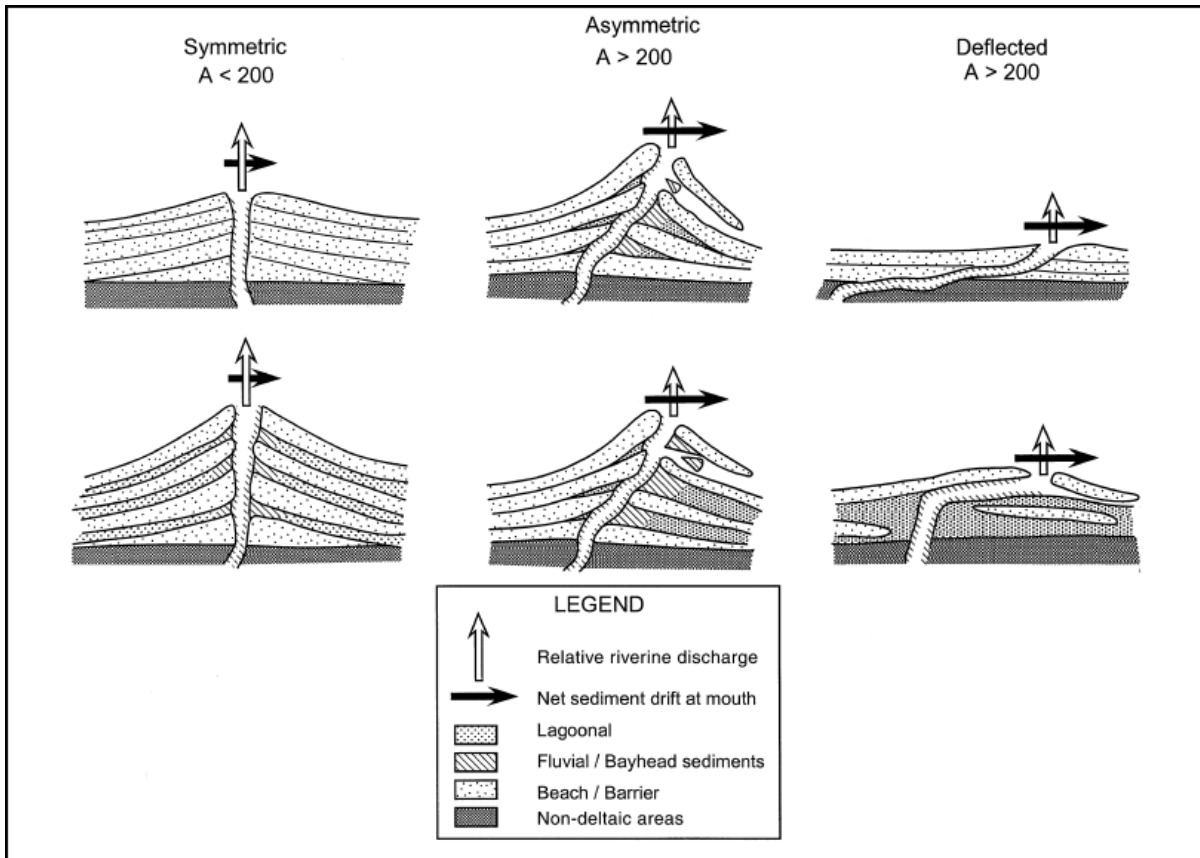
This figure is included on page 124 of the print copy of the thesis held in the University of Adelaide Library.

**Figure 3.4. Sandbody types and their average dimensions in deltaic systems.** The Flounder Field has been added to show its size relative its depositional systems (incised valley and TST shoreline). The delta and the division into upper (fluvial-dominated) delta plain and a lower delta plain are not to scale. Modified from Reynolds (1999).

NOTE:

This figure is included on page 125 of the print copy of the thesis held in the University of Adelaide Library.

**Figure 3.5. Width vs. thickness of shoreline-shelf sandbodies less than 50 km wide.** The differentiation by systems tract highlights the importance of identifying the systems tract if this type of data is to be used as an analogue when building 3D geological models. From Reynolds (1999).



**Figure 3.6. The interaction between longshore drift, fluvial discharge and fluvial sediment type.** Fluvial derived fine sediment is deposited in lagoons between beach ridges adjacent to the river. The relative strength of the longshore drift and the fluvial discharge influence the morphology of the delta. In asymmetric deltas, well data could give the appearance of a strandplain on the updrift side of the river mouth and a delta adjacent to and downstream of the channel. From Bhattacharya and Giosan (2003).

## NOTE:

This figure is included on page 127 of the print copy of the thesis held in the University of Adelaide Library.

**Figure 3.7. Potential modern analogues for the lower Roundhead Member.** A comparison of the size of the Gippsland Basin fields compared to the Nayarit Coast of West Mexico (top) and the east coast of Brazil (bottom). Either of these modern shoreface systems may be of comparable size to the system that produced the Gippsland Basin. The Flounder Field fits comfortably into a small portion of the Nayarit coastline or the Jequitinhonha delta. This diagram highlights the difficulty in distinguishing between strandplain and wave-dominated deltaic sediments in wellbore data. It is possible for the entire Flounder Field to sit within a strandplain associated with a delta and not penetrate any significant fluvial sediments. Nayarit Coast from Landsat images, Brazil Coast from Walker and Plint (1992).

NOTE:

This figure is included on page 128 of the print copy of the thesis held in the University of Adelaide Library.

**Figure 3.8. Mouth of the River Doce, Brazil.** Palaeo distributary channels (yellow arrows) can be seen to the north and south of the current distributary channel. The northern palaeochannel is adjacent to relic beach ridges, as is interpreted in the lower Roundhead Member. The southern palaeochannel can be seen to be terminated by more recent beach ridges—indicating reworking of the channel sediments close to the shore. The main distributary channels are approximately 1000 m wide, while the small channels (yellow star) are approximately 200 m wide—a similar width range to the interpreted width of the channel belts in the lower Roundhead Member. Image courtesy of NASA.

NOTE:  
This figure is included on page 129 of the print copy of  
the thesis held in the University of Adelaide Library.

**Figure 3.9. Barrier island formation through spit detachment.** Modified from Hoyt (1967).

NOTE:  
This figure is included on page 129 of the print copy of  
the thesis held in the University of Adelaide Library.

**Figure 3.10. Barrier island formation through the drowning of beach ridges during relative sea level rise.**  
As sea level rises, water ponds in the area between dunes and beach ridges, forming shallow lagoons that overlie coastal sediments. Modified from Hoyt (1967).



NOTE:

This figure is included on page 130 of the print copy of the thesis held in the University of Adelaide Library.

**Figure 3.11. Barrier island formation via bar emergence.** Waves breaking on an offshore bar gradually build up the bar to the point at which it becomes subaerially exposed. Barriers and lagoons formed by this method should overlie open marine sediments. Davis (1994) states that modern studies of barriers indicates that this method of formation is possibly the most common method of barrier formation. Modified from Hoyt (1967).

NOTE:

This figure is included on page 131 of the print copy of the thesis held in the University of Adelaide Library.

**Figure 3.12. Formation of transgressive barrier islands on the Mississippi delta front.** Reworking of distributary sediments forms transgressive barrier islands once the delta lobes abandoned. Continuing relative sea level rise further erodes the barrier. Modified from Penland et al. (1988).

NOTE:

This figure is included on page 132 of the print copy of the thesis held in the University of Adelaide Library.

**Figure 3.13. Elements of a transgressive barrier island system.** In this model the barrier deposits overlie lagoon sediments. Modified from Reinson (1992).

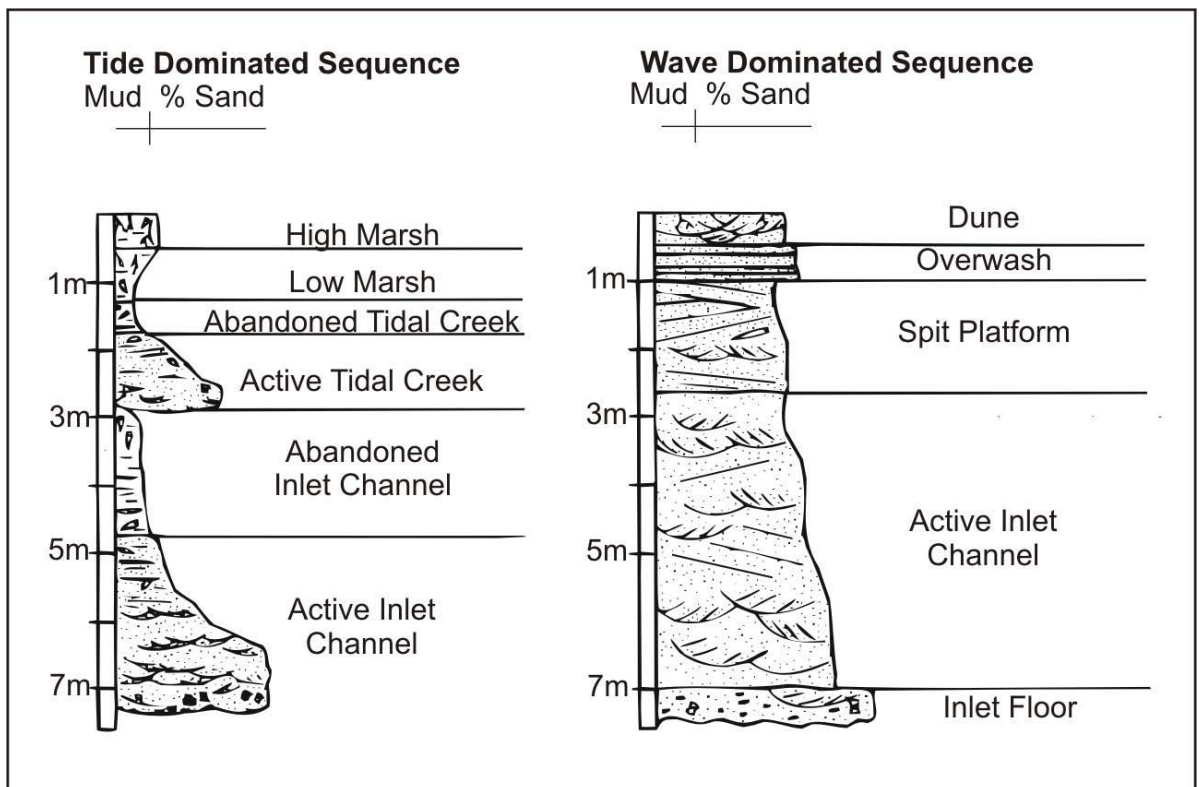
## NOTE:

This figure is included on page 133 of the print copy of the thesis held in the University of Adelaide Library.

**Figure 3.14. Part of the Gippsland Lakes barrier island system, Victoria.** The Gippsland Lakes are an example of a barrier island system in a wave-dominated setting. Prior to human intervention, tidal inlets formed during storms and were rapidly sealed during quiet weather by longshore drift (Bird, 1993). The lagoon was dominantly a fresh water system. Three generations of barriers can be seen in the Gippsland Lakes (A, B & C). The Prior Barrier (A) formed prior to the closure of the Gippsland Lakes. Note the palaeo tidal inlet and flood tidal delta (*ti*) adjacent to the Inner Barrier (B). Image courtesy of NASA.

**Figure 3.15. Tide-dominated barrier island system. east of Corner Inlet, Victoria.** This system has the short "drumstick" shaped barriers typical of tide dominated systems. The lagoon is shallow and highly channelized. The ebb tidal deltas can be clearly identified by the breaking waves (white lines). A complex network of tidal channels exists within the lagoon. Image courtesy of NASA.

NOTE:  
This figure is included on page 134 of the print copy of the thesis held in the University of Adelaide Library.



**Figure 3.16. A comparison of the deposits found in tide- and wave-dominated tidal inlets.** Tide-dominated inlets tend to be stable over a period of time and abandonment is via bar-bypass processes. This results in a mud plug overlying the channel deposits. Wave-dominated tidal inlets migrate relatively and the inlet channel is filled with reworked ebb-tidal sands (Moslow and Tye, 1985). Figure from Moslow and Tye (1985).

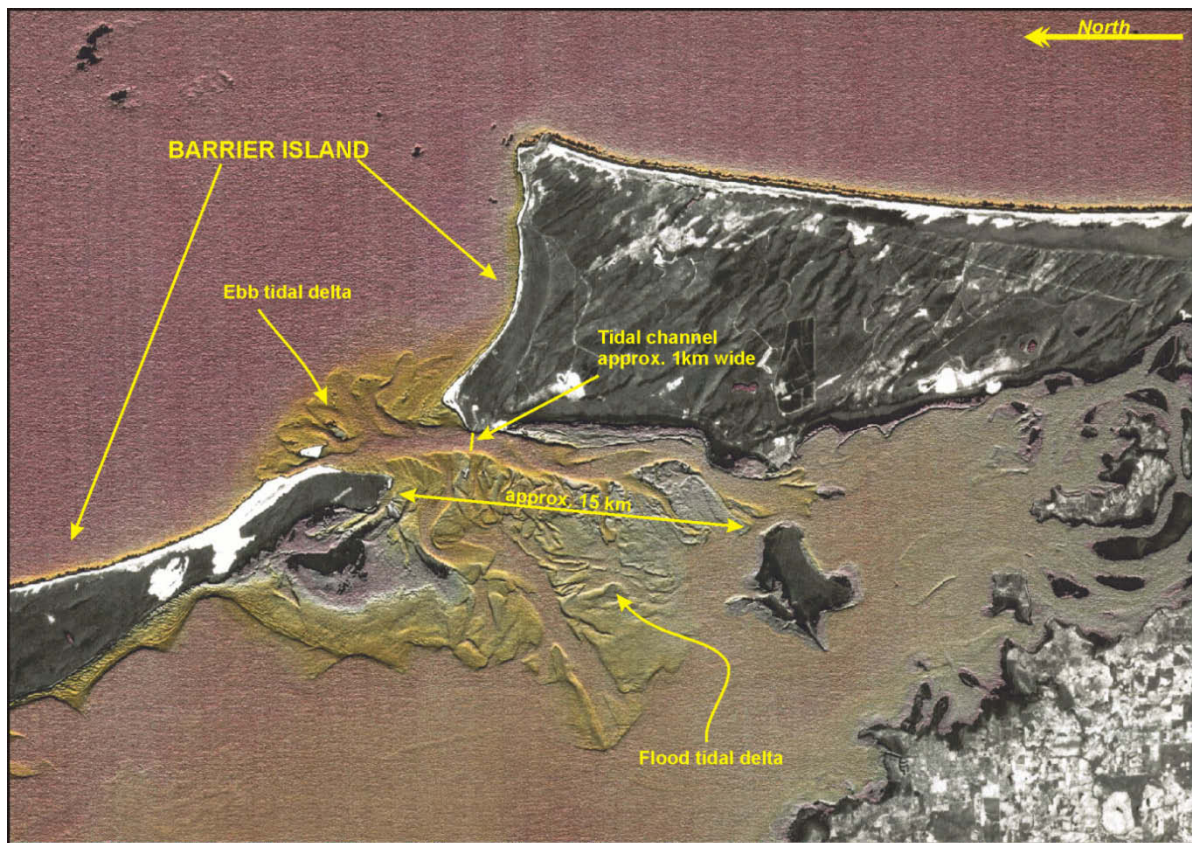


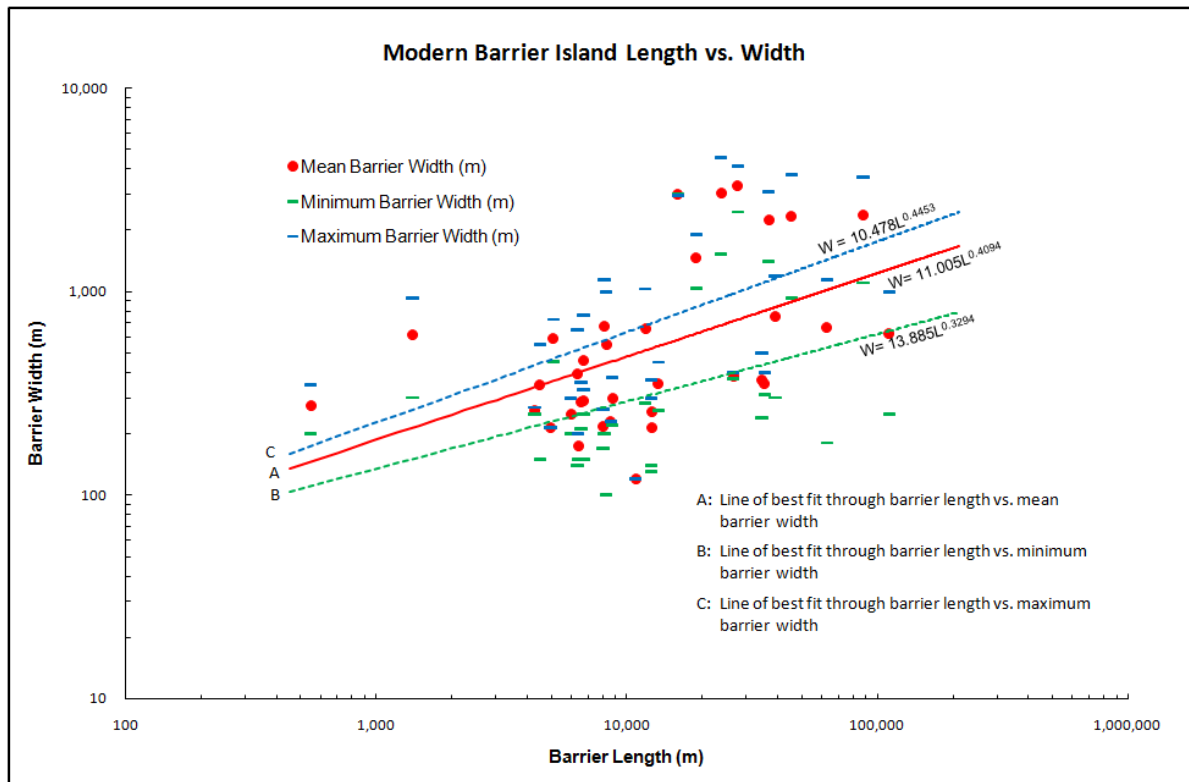
Figure 3.17. Modified Landsat image showing tidal-delta complex, Moreton Bay, Queensland. Image courtesy of S. Lang.

NOTE:

This figure is included on page 137 of the print copy of the thesis held in the University of Adelaide Library.

**Figure 3.18. Washovers on Dauphin Island, Gulf of Mexico after Hurricane Katrina.** The top two lidar images show changes in elevation after Hurricane Ivan (top) and Hurricane Katrina (middle). Green represents an increase in elevation and red indicates a decrease in elevation. The red squares represent destroyed houses. Hurricane Katrina resulted in a significant movement of sand off the barrier and into washovers in the lagoon (Mississippi Sound). From USGS/NASA (2005).



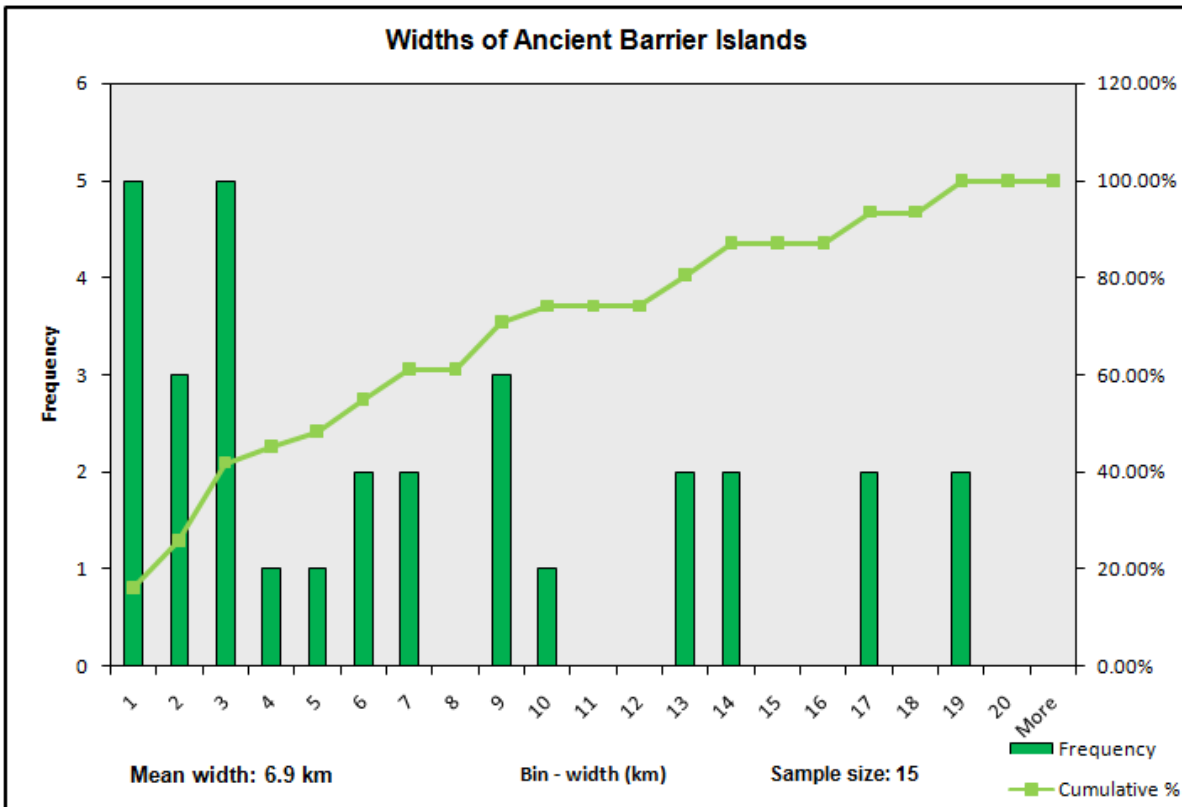
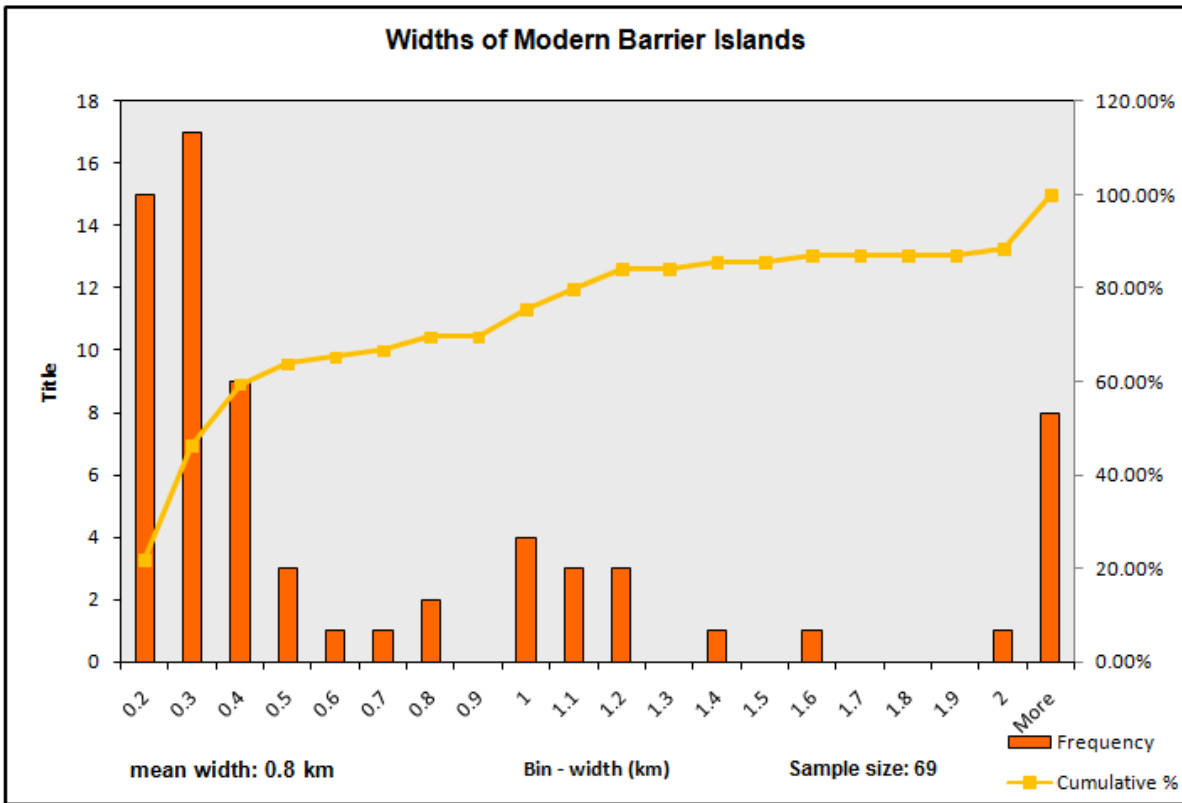


**Figure 3.19. Length vs. width of modern barrier islands, measured off Landsat images.** This chart does not distinguish between long narrow wave-dominated barrier islands and the shorter, wider tide-dominated barrier island systems. Such distinctions are unreliable from satellite images alone as not all barriers can be neatly pigeonholed or behave in the expected manner.

NOTE:

This figure is included on page 139 of the print copy of the thesis held in the University of Adelaide Library.

**Figure 3.20. Cross section through Roanoke Island and Outer Banks, North Carolina.** Seven stacked sequences are mapped, with DS-7 being the youngest, current coastal system. Each system has migrated upward and landward in response to the ongoing interglacial sea-level rise. The section highlights how little of a barrier system is visible on the surface relative to the overall width of the barrier deposit. Modified from (Riggs et al. (1992).

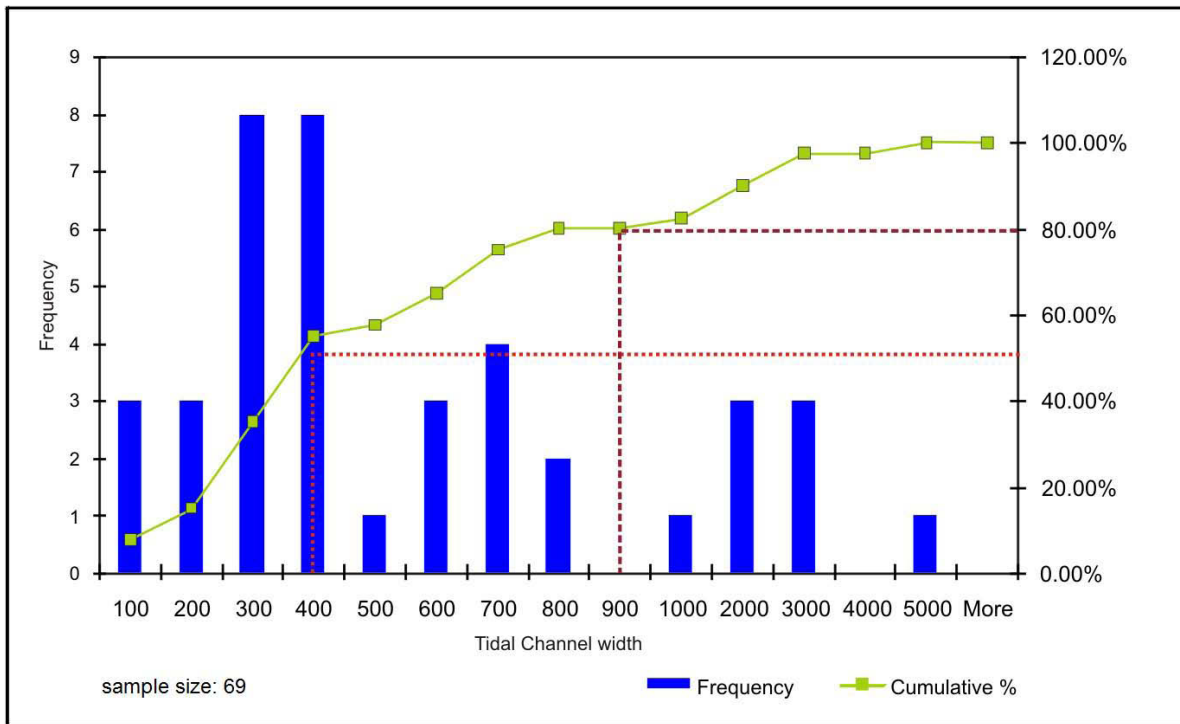


**Figure 3.21. A comparison of the widths of modern and ancient barrier islands.** Modern data was measured off Landsat images (Australia, Europe and USA), whilst ancient data was collected from a variety of published sources.

NOTE:

This figure is included on page 141 of the print copy of the thesis held in the University of Adelaide Library.

**Figure 3.22. Length vs. width of flood tidal delta complexes.** The plot shows a linear regression curve with correlation coefficient. There is a low correlation between the thickness of the flood tidal delta deposits and length or width. Eleven of these data points occurred in the transgressive systems tract. From Reynolds (1999).



**Figure 3.23. Frequency plot of tidal channel widths.** Data is estimated from Landsat images of tidal channels around the world. 50% of the tidal channels measured are less than or equal to 400 m wide. Widths are estimates only due to the resolution of the Landsat images and the difficulty in identifying man-made influences on channel properties.

NOTE:

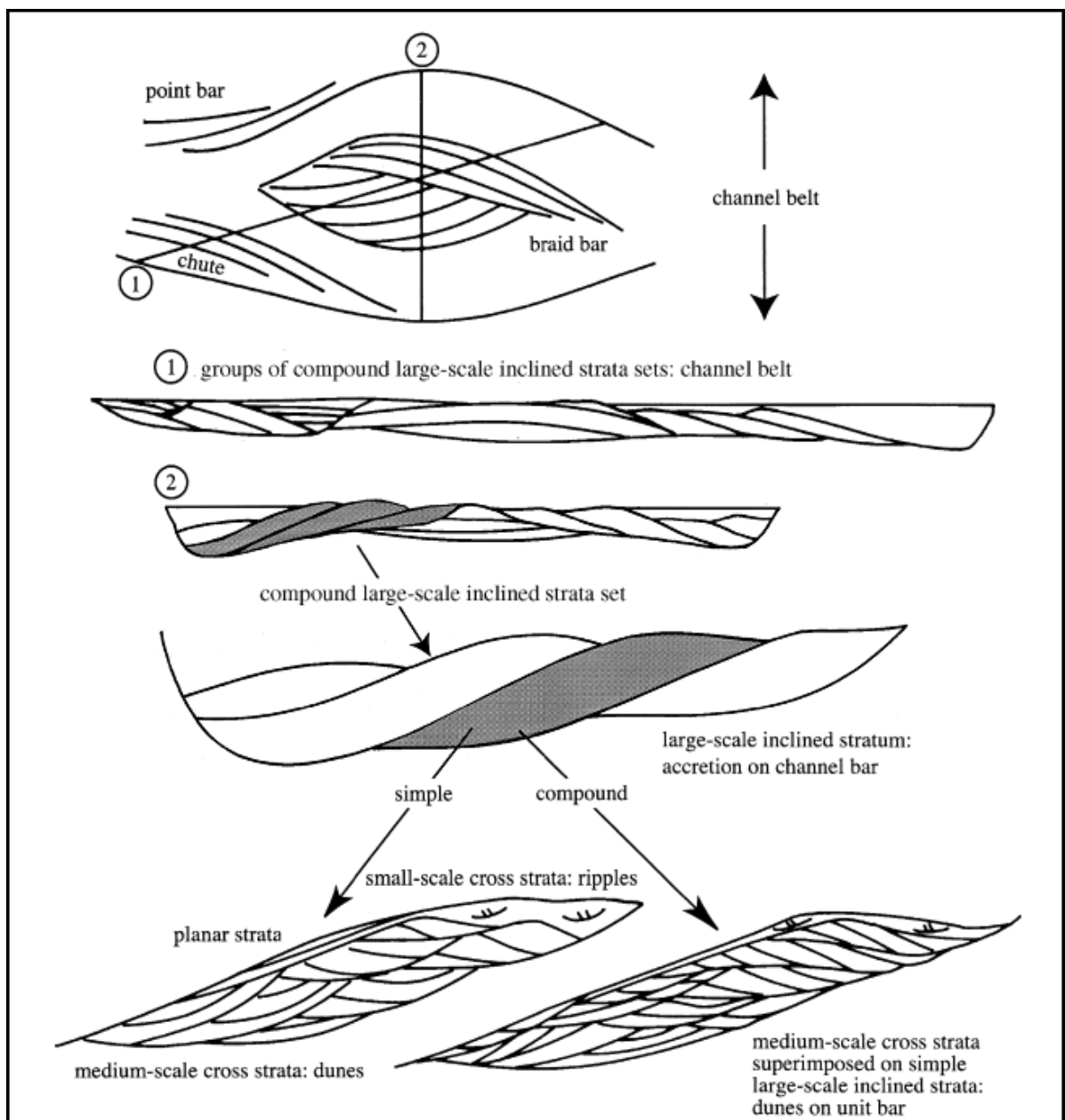
This figure is included on page 143 of the print copy of the thesis held in the University of Adelaide Library.

***Figure 3.24. Block diagrams showing the differences in sedimentation patterns between high sinuosity channels (A) and low sinuosity channels (B). Modified from Davies et al. (1993).***

NOTE:

This figure is included on page 144 of the print copy of the thesis held in the University of Adelaide Library.

**Figure 3.25. Yukon River, Alaska.** A low sinuosity fluvial system that is a potential analogue for the style of deposition seen in the upper Roundhead RU.1 unit. The active channels range from approximately 300–800 m wide. The active channel belt width is approximately 5 km. The amalgamated channel belt system is approximately 10 km wide. Longitudinal bars range from a few hundred metres to 5 km long and up to 2 km wide. Note the complex internal geometries of the abandoned lateral bars and segments of point bars on the alluvial plain (centre). This river has behaved as a braided river at different flow stages. The adjacent flood plain on either side comprises a veneer of floodplain sediments over remnants older alluvial deposits. Flow is towards the bottom of the picture (Riordan et al., 2006). Landsat image courtesy of NASA.



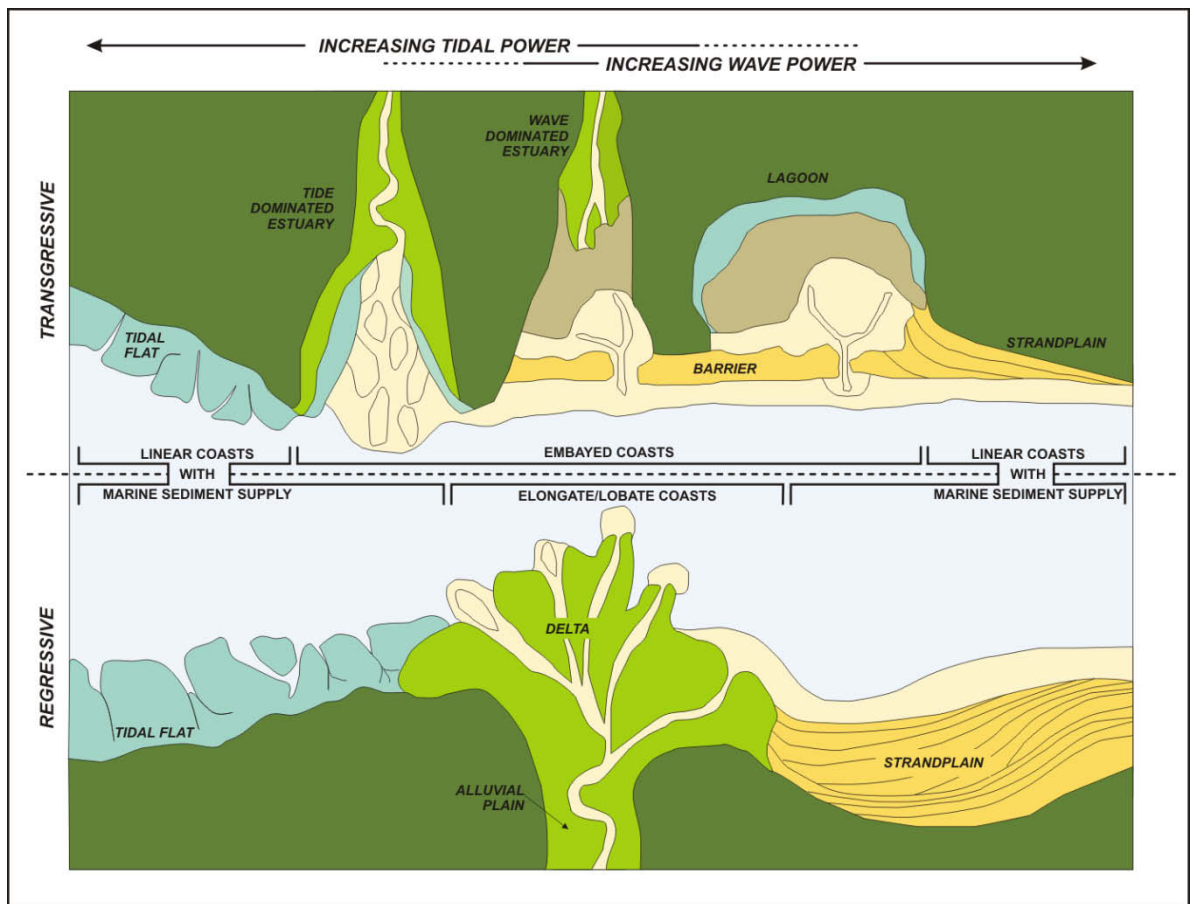
**Figure 3.26. Different scales of river channel deposits.** The top diagram shows an idealized channel belt hundreds to thousands of metres wide and metres thick. The channel belt is made up of groups of large-scale strata sets (1) & (2), which are tens of metres in length and decimetres thick. A compound large scale strata (shaded) set is made up of multiple accretions which can be formed in a single flood (simple) or be deposited over more than one flood event (compound). From Lunt et al. (2005), after Bridge (1993).



NOTE:

This figure is included on page 146 of the print copy of the thesis held in the University of Adelaide Library.

**Figure 3.27. A comparison of the depositional facies and their distribution between a wave-dominated delta (top) and a tide-dominated delta (bottom).** The deltas in a wave-dominated estuary are shielded from the influence of wave reworking by the presence of the barrier at the mouth of the estuary. The central basin mudstones are frequently highly bioturbated, but may show signs of stressed fauna associated with a brackish environment. Modified from Dalrymple et al. (1992).

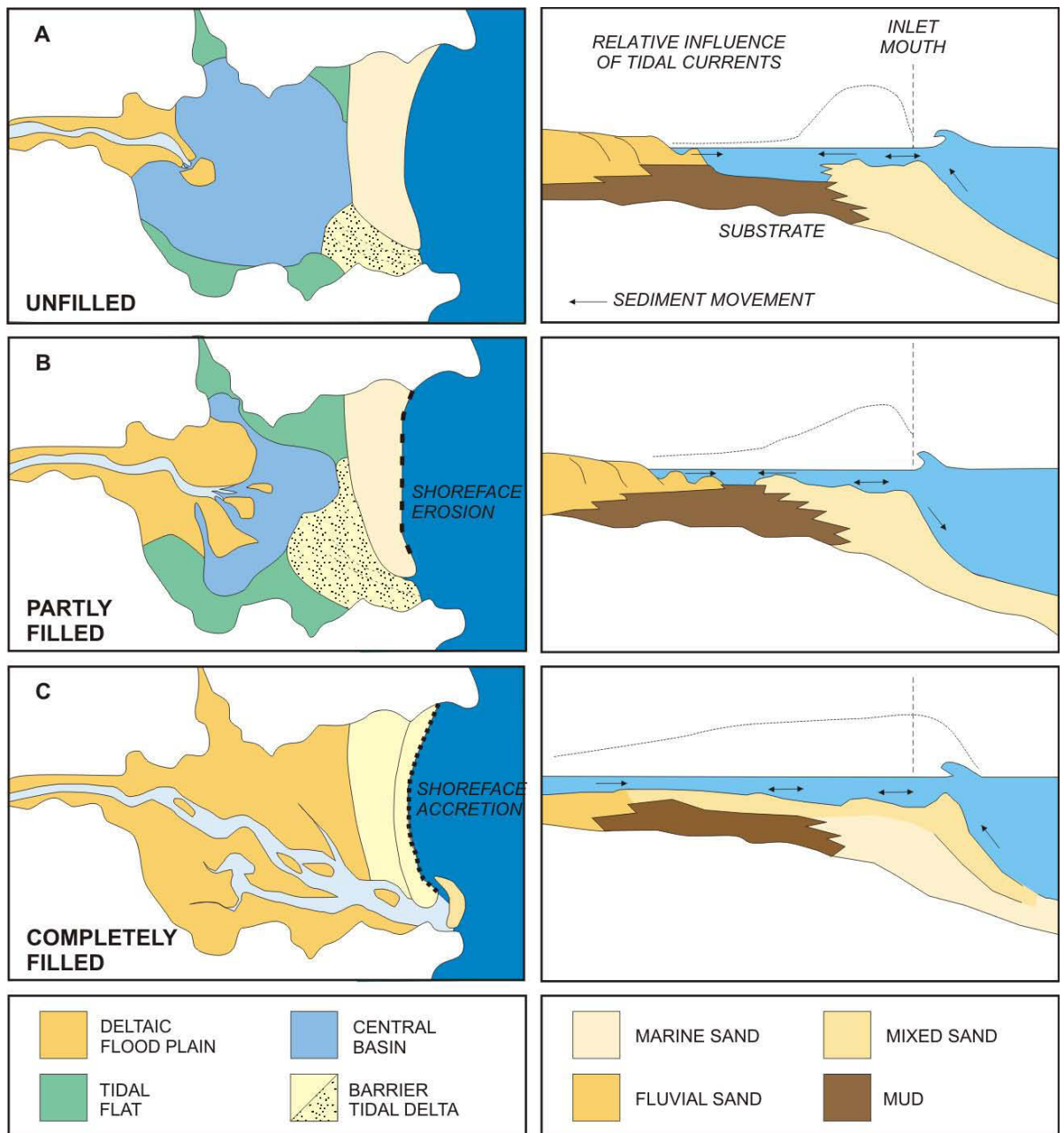


**Figure 3.28. Classification of coastal environments.** This diagram highlights the differences between wave-dominated estuaries and lagoons. Modified from Boyd et al. (1992).

NOTE:

This figure is included on page 148 of the print copy of the thesis held in the University of Adelaide Library.

**Figure 3.29. Elements of a wave-dominated estuary.** This diagram highlights the energy associated with each part of the estuary. The bottom diagram highlights the juxtaposition of facies in this facies model. Although the barrier shoreface is transgressive, and overlies more landward facies, the fluvial elements are prograding into the estuary at the same time. Modified from Dalrymple et al. (1992).



**Figure 3.30. Changes in depositional facies distribution as a wave-dominated estuary is filled.** As the estuary fills, the relative influence of tidal currents penetrates further inland, and bidirectional cross-bedding becomes more widespread. Note the change in shape of the bayhead delta from a funnel shape during the early stages of estuary fill (A), to a more distributive pattern as the estuary fills (B). Once the estuary is filled (C) it is regarded as a delta as fluvial deposition is occurring on the shoreface. Modified from Roy et al. (1980).

NOTE:

This figure is included on page 150 of the print copy of the thesis held in the University of Adelaide Library.

**Figure 3.31. Superimposed channel bars and channel belts within a single channel belt complex.** This highlights the difficulty in identifying individual channels from wireline logs for thickness/width calculations. There is a high degree of likelihood that channel depths will be overestimated where younger channels have eroded the channel abandonment phase of older channel deposits. In low sinuosity systems where there is unlikely to be a significant fining-upward log signature in the first place, this becomes even more difficult. From Bridge and Tye (2000).

NOTE:

This figure is included on page 151 of the print copy of the thesis held in the University of Adelaide Library.

***Figure 3.32. Channel depth to channel belt width ratios, showing Upper roundhead RU.1 unit dimension.***

The width:depth ratio used is case 2A, as the low sinuosity data are highly scattered. This is very different from the braided stream data (blue ellipse) which are more concentrated, and would have a higher ratio.

Case 2A, the best fit for all data collected was found by Robinson and McCabe (1997) to closely approximate the average regression line for the braided stream deposits of the Salt Wash Sandstone Member, Utah. Modified from Fielding and Crane (1987).

**Figure 3.33. Width:thickness plot for incised valleys with alluvial and marine strata.** The width of the RU.1 unit incised valley, as shown of the palaeogeographic diagram (Figure 2.42) has been added to the plot. This indicates that the maximum thickness of the incised valley (approximately 20 m) is comparable to other data points. The width of the valley could be anywhere from 5 to 20 km and remain within the limits of the dataset examined by Gibling (2006). Modified from Gibling (2006).

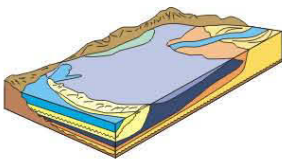
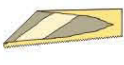


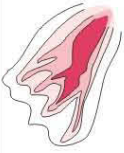
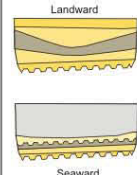
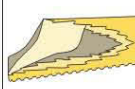
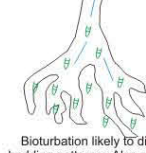
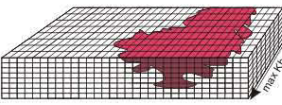
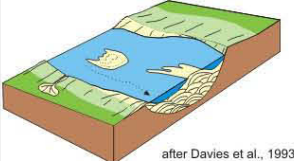

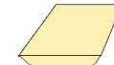




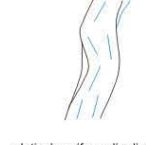
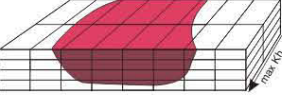

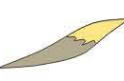

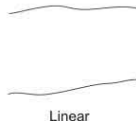
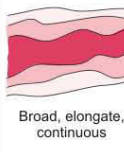

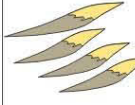
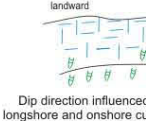
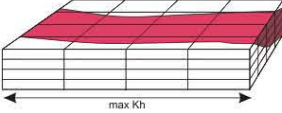
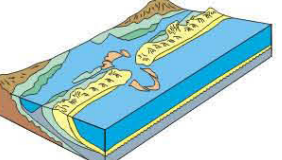


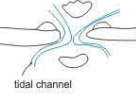


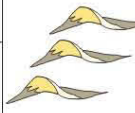
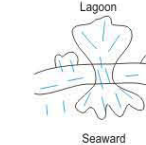
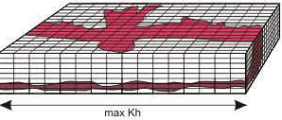
NOTE:  
This figure is included on page 152 of the print copy of  
the thesis held in the University of Adelaide Library.

NOTE:

This figure is included on page 153 of the print copy of the thesis held in the University of Adelaide Library.

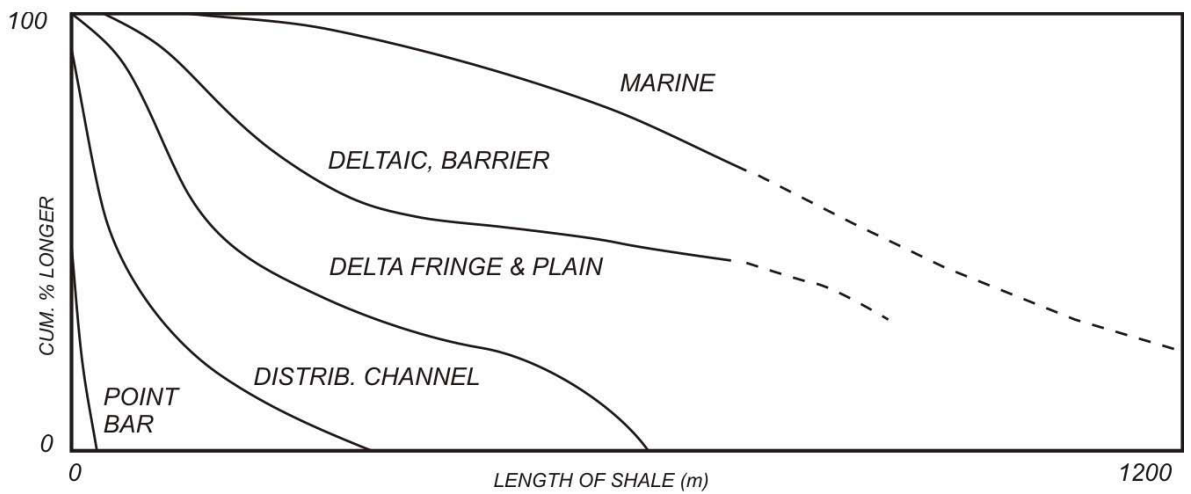
**Figure 3.34. Fluvial stacking patterns and their relationship to systems tracts.** From Posamentier and Allen (1999).



depositional feature	depositional system features	geometry of depositional feature	cross section	sand body geometry			lateral relationships	maximum horizontal permeability orientation	range of dimensions	Idealised grid cell geometry
				plan view	sand isopach	bedding character (architecture)				
bayhead delta in wave-dominated estuary		 Upwards fining sand, overlain by mud, followed by upwards coarsening sand	 width/thickness ratio 10-1000*	 ranges from funnel shape to birdfoot - depending on relative influence of tide and river		 Landward Seaward	 ratio of central basin muds to sand varies with position in estuary	 Bioturbation likely to disrupt bedding patterns. Also potential for tidal mud drapes.	Bayhead Delta Length: 1-10s km Width: 1-10s km	
low sinuosity (bedload) fluvial channels	 after Davies et al., 1993.	 Blocky, homolithic (dominantly sand)	 width/thickness ratio 50-1000*	 straight or low sinuosity		 vertical accretion dominates	 channel fill volumetrically exceeds overbank deposits (channel sand = 65%)	 relatively uniform dip direction - consistent preferred permeability orientation	Meander Belt Length: 10s-100s km Width: 1-10s km	
Strandplain		 Upwards coarsening, heterolithic (increasing sand content landward)	 thickness/length: 1:10000 <sup>^</sup> thickness/width: 1:1300 <sup>^</sup>	 Linear		 gently dipping, shore parallel beds. Longshore drift vs. onshore will influence depositional dip	 Highstand shoreline wider than transgressive shoreline	 Dip direction influenced by longshore and onshore currents - level of complexity related to current/climatic conditions. bioturbation offshore disrupts bedding planes	Shoreline Length: 10s-100s km Width: 1-10's km	
Barrier Island Complexes	 after Reinson, 1992.	 Variable sand distribution, marine and lagoon shales surround the sand	 width/length ratio 1:25 <sup>^</sup>	 tidal channel Complex pattern of shoreface, tidal delta, tidal channel, washover and lagoon sediments.	 Complex, dependant upon frequency of tidal channels and washover fans.	 gently dipping shoreface sediments, lagoonward washover fans and flood tidal deltas. tidal channel cut through all, and may be sand or shale filled.	 Rapid sea level rise drowns barrier in place	 Lagoon Seaward Highly variable dip direction due to multitude of depositional features - complex preferred permeability orientation	Barrier Island Length: 1-10s km Width: 100s m	

\* from Gibling (2006) common range  
<sup>^</sup> from Reynolds (1999) - mean values  
<sup>o</sup> from Landsat image measurements - mean values

**Figure 3.35. A comparison of fluvial and shoreface deposits.** This diagram highlights the differences in sandbody size and distribution between the depositional environments seen in the Flounder Field. When building 3D models of these environments the differences in sandbody size and distribution need to be considered during the early stages of grid design, through to the population of the grids, and beyond to upscaling for reservoir simulation. Low sinuosity channels panel after Davies et al. (1993).



**Figure 3.36. Lateral shale continuity as a function of depositional environment.** This graph indicates that shales in marine and deltaic deposits are likely to form significant flow barriers. Although shales in fluvial systems are unlikely to form field wide barriers, they will have a major influence on the permeability of the reservoir. From Haldorsen and Lake (1984), after Weber (1980).



## 4 STATIC MODELS

### 4.1.1 Key terms

- Scenario                    facies & petrophysical model combination
- Realization                equiprobable arrangement of facies that conforms to a set of input parameters
- Grid Design                grid block dimensions and number of layers
- Cell size                    the x and y dimensions of the cells
- Layer size                  the number of layers in the grid
- Model                        the combined package of cell size and layer size
- Grid Orientations        square (SQ), shoreface strike aligned (SSA) & shoreface dip aligned (SDA)
- Base Model                The initial model, where the facies and petrophysical models were built, prior to upscaling
- 200 x 160 x 24            Refers to the model with 200 x 160 cells and 24 layers. Where cell dimensions are discussed in meters, it will be highlighted or in brackets.

## 4.2 Introduction

This chapter describes the how 3D geological models were constructed in this project. The construction of modern 3D geological models aims to incorporate interpretations of depositional environments, seismic attributes, petrophysics and reservoir engineering data that helps to define flow units and sandbody connectivity (Pelgrain de Lestang et al., 2002; Tye, 2004). Summaries of the procedure for building models include Begg et al. (1992), Bryant and Flint (1993), MacDonald and Aasen (1994), Galli and Beucher (1997), Cook et al. (1999), Marion et al. (2000), Larue and Legarre (2004), Keogh et al. (2007) and Howell et al. (2008). A common feature of case studies of 3D modelling projects is that they generally give very little detail of cell dimensions and the thought processes behind the choice of the cell dimensions. Exceptions include Cook et al. (1999) and Ainsworth (2005). Furthermore, it is hard to find examples where multiple upscaled cell sizes have been used and dynamic

simulation results compared and related back to a geological model. Zhang et al. (2007) examines many upscaled models of different sizes but do not relate the results back to the width of the channel being modelled. Tegnander and Gimse (1998) upscaled a permeability model horizontally and vertically to different cell sizes, and found a poor correlation between the base grid and the majority of the upscaled grids, but did not relate the final results back to the distribution of the permeability in the base grid. The figures provided by Tegnander and Gimse (1998) suggest that many of the upscaled grids may have been larger than the facies bodies modelled both horizontally and vertically. Haajizadeh and Begg (1993) showed that in a 2D model vertical upscaling always reduced ultimate recovery and brought forward the time to waterflood breakthrough. Horizontal upscaling generally reduced the ultimate recovery and brought forward water breakthrough. Haajizadeh and Begg (1993) also found that models with cells sizes that were the same as significant heterogeneities were less reliable than models with smaller or larger cells.

Authors such as Carlson (2003) and Zhang et al. (2005) allude to the inaccuracy of reservoir simulation results if permeability heterogeneity, especially in channel models, is not preserved, but once again tend not to relate discussions of heterogeneity in terms of sandbody dimensions.

The aim of this study was to determine if sandbody dimensions influence the point at which reservoir heterogeneity is lost, and if so does it result in a predictable loss of reliability of simulation results.

The 3D modelling component of this thesis was carried out using Roxar's RMS version 7.4 and 8.0 software. A series of facies models were built, upscaled and then dynamic modelling was carried out using the FlowSim module of RMS. Two generations of models were built as the requirements of the models were refined (Figure 4.1).

The first generation of facies models aimed to match, as closely as possible, the interpreted well data. The facies and petrophysical models honoured the well data, and were used to build variogram models for the various environments in this field. During the construction of

---

these models, properties such as angles of shoreface progradation that can only be fully understood by building 3D models that honour the well data were interpreted.

The second generation of facies models used the distributions and dimensions identified in the first series of models, but did not honour the data at the well bore. These conceptual models will be referred to as the 'base models' from this point. By not honouring the data at the well bore, the time taken to build models was significantly decreased, and volumes of facies such as channels could be easily altered to study the effect on the upscaling process.

Three different grid orientations were used so that the influence of cell shape on upscaled facies models could be studied (Figure 4.1). For each grid orientation, five geological scenarios were built and simulated. The same upscaling process was carried out for all grid orientations. The base models and their upscaled derivatives were compared to identify facies-based changes to porosity distribution and pore volumes that occur as the grids are upscaled. Reservoir simulation was then carried out on selected models to determine if the changes identified in the static models influence the results of reservoir simulation in a predictable manner.

## 4.3 Methodology

### 4.3.1 Grid Design

Three grid designs were constructed in order to assess the influence of grid orientation on upscaling results (Figure 4.2). The grid orientations were as follows:

- Square (SQ) – grid blocks were approximately equal length in the x and y axes
- Shoreface Strike Aligned (SSA) – grid blocks were longer in the x-axis than the y-axis
- Shoreface Dip Aligned (SDA) – grid blocks were longer in the y-axis than the x-axis

The shortest side of the SSA and SDA grids was approximately the same length as the sides of the square grid, while the longest sides were approximately twice the length of the square

grid. The x-axis on models is rotated 40° to the normal (East). This was so that the grids were aligned with the interpreted orientation of the palaeo-coastline in the Flounder Field. All grids were corner point grids (Ertekin et al., 2001). As there were no grid refinements around the wellbores, the cell dimensions were consistent across the model.

All conceptual models were built between the RL.6 surface (top) and the RL.3 surface (base) (Figure 4.3). The RL.3 surface is the only lower Roundhead surface that is found in all wells, and is picked on a flooding surface that is present in most wells (Figure 4.3). The RL.6 unit is present in all wells except Flounder 2, where the overlying sequence boundary cuts into the top of RL.5. This area of erosion is interpreted to be relatively small and the isopach of the top RL.6 to top RL.3 interval is dominated by facies distribution rather than erosion/onlap. As a result the models were built with 24 proportional layers which are evenly spaced between the top and bottom surface. The average thickness of the layers is 0.5m. In order to reduce complexity, the numerous faults that were interpreted in the Flounder Field were not imported into the 3D model. The surfaces used to build the model reflect the structure of the Flounder Field, without imposing the influence of faulting on the behavior of the dynamic models.

## **4.4 Facies Models**

Two methods were used for building the facies models. Depositional elements that migrated across the field, such as shorefaces, were modelled using the RMS facies modelling 'belt' module (Roxar, 2005) (Figure 4.4). This module uses a truncated Gaussian simulation algorithm to model features, such as shorefaces, by laterally offsetting facies belts. This method required the definition of the relationship of the shoreface to adjacent facies, the accretion angle, belt width, belt orientation and amount of interfingering (MacDonald and Aasen, 1994). The boundaries of the belts are modelled stochastically while honouring the well data.

Elements deposited in channels, such as tidal channels and fluvial channels were modelled using the RMS facies modelling 'channels' module. This uses object modelling techniques to

---

model discrete channels in a background facies. This method required input of channel volume, channel dimensions, sinuosity and orientation.

Both the facies and porosity models were populated using stochastic modelling (Roxar, 2005). Where necessary the individual elements were merged together to form a complex depositional system (Figure 4.4). For each of the three grid designs, the same input parameters were used in the building of the facies and porosity models for each scenario.

#### 4.4.1 1<sup>st</sup> Generation Models

##### 4.4.1.1 Upper Volador Barrier Island

A model was built of the upper Volador barrier-island system of the VU.2 to VU.0 units (Figure 4.5). This interval is unaffected by erosion associated with SB1, and is modelled with an even number of layers across the field (average 0.5 m thick). The facies model built was simple, consisting of four facies: offshore, barrier shoreface, tidal channel and lagoon. Washover fans and tidal deltas are not modelled discretely but incorporated into the barrier island facies, as it was difficult to identify them on the wireline logs away from the very limited core data (cored in one well, and one core sample taken in this interval). The landward side of the barrier facies has a more undulating boundary than the seaward edge of the barrier to approximate the washovers and tidal delta sediments which incorporated in the barrier facies. Tidal channels were identified by an upwards-fining wireline signature. The distribution of the tidal channels on the log signature plots indicates that they were narrow and do not appear to migrate laterally a significant distance. The stable nature of the channels is consistent with the interpretation of a tide-dominated barrier-island system. The tidal channels are modelled cutting through the barrier shoreface but do not penetrate into the lagoon or offshore facies. The dimensions of the sandbodies in the upper Volador Formation barrier islands were derived from a variety of sources. The width of the tidal channels was interpreted from the log signature plots (approximately 600 m). The width of the barriers was determined by getting a best fit of the barrier boundaries to a layer by layer breakdown of the well data. Although the preserved amalgamated barrier-island/tidal delta



complex is inferred to be between 1 and 3 km wide, the barriers are between 400–1200 m wide on any given layer in the model (Figure 3.1). This is within the range of widths of modern barrier islands as measured from Landsat images. The average width of individual tidal channels in the geological model is 600 m. This width is also within the range of modern tidal channels seen on Landsat images. The log signature plots do not indicate that the channels underwent significant lateral migration, making the widths of modern channels a good reality check for the model dimensions.

#### ***4.4.1.2 Lower Roundhead Strandplain Model***

The lower Roundhead was modelled for the interval between the top of the RL.6 and RL.3 units (Figure 2.33). This interval is present in its entirety in the majority of wells in the field. The interval has an average thickness of 12 m, and the model contains 24 layers which have an average thickness of 0.5 m. The facies modelled were offshore, shoreface, channels and coastal plain. As indicated by the palaeogeographic maps, the shoreface widens and progrades through time (Figure 2.33). The seaward shoreface boundary migrates seaward at a faster rate than the landward boundary. The shoreface at the base of the model (top of RL.3 unit) is approximately 1900 m wide. The width of the shoreface increases evenly through the model, and at the top of the RL.6 unit it is approximately 3300 m wide (Figure 4.6). As with the barrier-island model, the width of the shoreface and the angle of inclination of the shoreface were established in RMS during the facies building process. A layer by layer analysis of the facies interpretation indicated that a progradation angle of 0.3 degrees for the shoreface/offshore boundary would provide the best match of the facies data. This value is comparable to angles of shoreface-shelf profile measured in the Book Cliffs by Hampson (2000), Hampson et al (2001), Hampson and Storms (2003) and Sixsmith et al (2008). Howell et al. (2008) define shoreface progradation angles of 0–0.3 as a low angle of aggradation, 0.5–0.8 as mid-range and 1.0–1.4 as high aggradation. MacDonald and Aasen (1994) used a range of aggradations angles between 0.05–0.2, and regarded an aggradation angle of 0.5 as high.

---

The facies model was constructed in several steps so that the final facies model has channels cutting into the shoreface but not connecting with the lower shoreface facies—implying that the fluvial channels were reworked at the shoreface as the coastal plain prograded, but preserved in the backshore (Figure 4.4).

As discussed in [section 2.8](#) it is uncertain whether the lower Roundhead Member was deposited on a strandplain or a wave-dominated delta. As the unit is being modelled as a strandplain with fluvial input, the channel facies is being modelled as low sinuosity channel belts with dimensions based upon Fielding and Crane's (1987) width to thickness plot. This indicated that the channel belt could have widths of 40–350 m (from a mean thickness 5 m). If the alternative interpretation of distributary channels on a wave-dominated delta were to be modelled, the width, orientation and porosity distribution within the channels would be different. The channel facies has a net:gross ratio of approximately 25% on the coastal plain. Channel models with a net:gross ratio of less than 30% are usually regarded as poorly connected (Larue and Hovadik, 2006), in which case fluid flow through the reservoir is likely to be dominated by channel connectivity rather than the internal porosity and permeability distribution of the channels (1990).

#### ***4.4.1.3 Upper Roundhead Fluvial Model***

The RU.1 unit was the only part of the Upper Roundhead to be modelled. This interval is the lowstand fluvial fill of the incised valley. Unlike the lower Roundhead and Volador models, the grid for the upper Roundhead was built using the even thickness, top down method in order to capture the onlapping nature of the basal part of the unit. As it is sand rich, the influence of channel dimensions on fluid flow is expected to be small. The net:gross of the upper Roundhead Member is such that the facies model of the unit resembles a blanket of sand with occasional pods of shale. Sand rich reservoirs with a net:gross >80% are regarded as having excellent connectivity (King, 1990; Bridge and Mackey, 1993; Larue and Friedmann, 2005; Larue and Hovadik, 2006). In this situation, it is expected that the influence on porosity distribution in upscaled models would be the variograms used to model porosity distribution.

#### **4.4.2 Conceptual Models (2<sup>nd</sup> Generation Models)**

Two types of conceptual facies models were built. They are a shoreface that represents the lower Roundhead Unit, and a fluvial channel model that represents the upper Roundhead Unit. These two systems were chosen as they are the 'end members' of reservoir connectivity and homogeneity of the environments interpreted in the Flounder Field. The geological models built are as follows:

- Strandplain:
  - a. Shoreface only ('beach' scenario),
  - b. Multiple channels intersecting the shoreface ('coast' scenario). Analogue of the RL.6-RL.3 interval.
- Channels Only:
  - a. 100 m wide, 25% by volume (100-25 scenario),
  - b. 100 m wide, 50% by volume (100-50 scenario),
  - c. 280 m wide, 25% by volume (280-25 scenario),
  - d. 280 m wide, 50% by volume (280-50 scenario).

When generating these facies models, the facies distribution is not tied to the well bores. Thus there is no guarantee that wells will intersect fluvial sandbodies in the channel models. The facies present in the channel scenarios are channel and overbank. Although the channels represent channel belts, they will be referred to simply as channels. The channels are oriented approximately perpendicular to the palaeocoastline. The channels are oriented such that the average strike approximates the strike of the long sides of cells in the SDA grid.

Two widths of channels were modelled as it was not possible to design one grid that would allow for all upscaling influences to be analyzed in one scenario. The 100 m channel scenario permits analysis of the simulation behaviour when cell size exceeds channel width, but gives little information about changes in results when the cell size is less than channel width. The 280 m model provides more information about the simulation behavior as cells are upscaled up to the channel width, but gives little reliable information about upscaling beyond the channel widths as well spacing rapidly becomes an issue. When there are three cells or

---

fewer between the injector and producer, simulation results are unreliable (Weber and van Guens, 1990). Expanding the area of the model so that the wells could be moved further apart was not practical as a) the grid is based on the area of the available structure map and b) a larger grid volume would mean that the grids with small cells would have too many cells for the available computers to simulate.

The coast scenario was built using the same parameters for the shoreface facies as the model of the lower Roundhead Member (1<sup>st</sup> generation), and 280 m channels. The beach scenario used the same elements as the coast scenario, but did not have the fluvial channels merged into the final model.

## 4.5 Petrophysical Models

### 4.5.1 Porosity

Porosity logs for all wells were included in the dataset acquired from ExxonMobil, and are used in the porosity models. In some situations very low porosity values have been edited to bring them in-line with a high gamma reading. Further petrophysical examination was beyond the scope of the thesis work and hence it is considered an acceptable assumption.

Porosity distribution was analyzed by facies in RMS. The porosity data were studied to establish ranges for variogram models for each facies in the coastal plain model. The orientation of the variograms (anisotropy direction) is related to the orientation of the sandbodies in each facies unit. The porosity anisotropy in the channel facies follows the curvature of the channel bodies, and in the shoreface facies it is parallel to the interpreted coastline (Figure 4.7). The variograms used to model the porosity distribution in the overbank (channel scenarios) and offshore and coastal plain facies (coast scenarios) are spherical, resulting in patchy porosity distribution that aims to emulate crevasse splay or storm deposits.

The petrophysical models applied arbitrary maximum porosity cut-offs to the overbank, coastal plain and offshore facies (10%) to ensure a significant difference between the 'reservoir facies' (shoreface and channel) and the 'non-reservoir' (overbank and offshore marine). The aim of this was to ensure that the 'reservoir' facies are the primary influence on fluid flow, thus enabling the influence of upscaling these facies to be studied. This distorts the total porosity distribution of the porosity models compared to the original log data (Figure 4.8). However, if the porosity distributions are filtered to show only the shoreface or channel facies they reflect the distribution of the original log data (Figure 4.9). The reservoir facies include very low porosity values as there is carbonate cement in sandstones in some wells. These anomalously low values have not been edited out of the data set but a low end porosity cut-off of 1% was applied to the data so that permeability could be calculated without creating permeability values of zero. The 'non-reservoir' facies have not been assigned zero porosity in order to maximize porosity contrast. This is in recognition of the fact that in gas-bearing reservoirs they can play a significant role in the long term production profiles, and thus their influence on upscaling needs to be understood.

#### **4.5.2 Permeability**

A relationship between permeability and porosity was determined from the core analysis data (air permeability at atmospheric pressure). No corrections for reservoir pressure or reservoir fluid have been applied. Two curves were used to create a permeability relationship with porosity. For the offshore marine and coastal plain facies the curve  $k = 0.01e^{48.807\phi}$  was used (Figure 4.10). As the porosity in the non-reservoir facies is restricted to values of 10% or less, the permeability in these facies will be below 20 mD. For the shoreface and fluvial channel facies the curve  $k = 2 \times 10^7 \phi^{5.9675}$  was used (Figure 4.10:B). This curve is based on the core plugs taken from shoreface facies. The permeability model in RMS was created by applying these relationships to the porosity model. A cut-off was then applied to the permeability parameter so that any values less than 0.001 mD were shifted to equal 0.001 mD.

---

### 4.5.3 Hydrocarbon Pore Volumes

Hydrocarbon pore volumes were calculated in RMS for each scenario and each grid design (Realizations 1–3). These are calculated for the whole volume and are also separated into facies. Graphing pore volume by facies highlights the changes in facies distribution as the grids are upscaled. The changes in pore volume will be compared to the results of the reservoir simulations to establish if the trends seen are indicative of the behavior of the dynamic models.

The volumes within the channel facies that are connected to the wells are also reported. These are calculated using RMS's geometric connectivity function. These volumes were also compared to the results of the reservoir simulations to establish if this property can be related to upscaling influences and reservoir simulation results.

## 4.6 Discussion – Static Models

Analogue data have been incorporated into the facies models in two ways. Ancient analogues have been used to provide an estimate of how wide fluvial channels may have been, based on published width to thickness ratios. The dimensions of modern analogues, such as shorefaces and barrier islands, have been measured from aerial images available on the internet from sources such as NASA and Google Earth. Modern data has been used as a guide to the widths of sandbodies, such as barriers islands, in individual layers in a facies model, whilst ancient data sets have been used to define ranges for the total size of sandbodies within the models. There are limitations to both these datasets as sources of sandbody dimensions. Dimension data associated with ancient analogues is generally amalgamated into a large collection of data of similar depositional origin, such as (Fielding and Crane, 1987; Reynolds, 1999; Gibling, 2006). Given the varying nature of outcrop exposures, such datasets rarely produce close relationships between length, width and thickness, so the user may need to choose values from a graph that may cover several orders of magnitude or use a combination of data sources.

Care also needs to be taken when acquiring and using dimensions measured from satellite images. While satellite images provide an excellent overview of a depositional system, it can be difficult to distinguish between natural features and those that have been altered by human activity (for example the widths of tidal inlets in barrier islands). The scale of satellite images also lends itself to analysis of large systems more easily than small systems whose features are close to the lowest resolution of the image. This has the potential to introduce a size related bias into the sampling process. Although satellite images allow the rapid acquisition of large volumes of length and width data, they provide no information about the thickness of systems. Some prior knowledge of the system being measured is also advisable as details such as grain size are not distinguishable, and it is for example, easy to mistake features such as cheniers for strandplains.

Where well control is good, analogue data may only be needed as a reality check to ensure that field based interpretations are within the realms of geological likelihood. In situations of poor well control, analogues should be used with caution—preferably as inputs for a variety of facies model scenarios.

## 4.7 Figures – Static Models





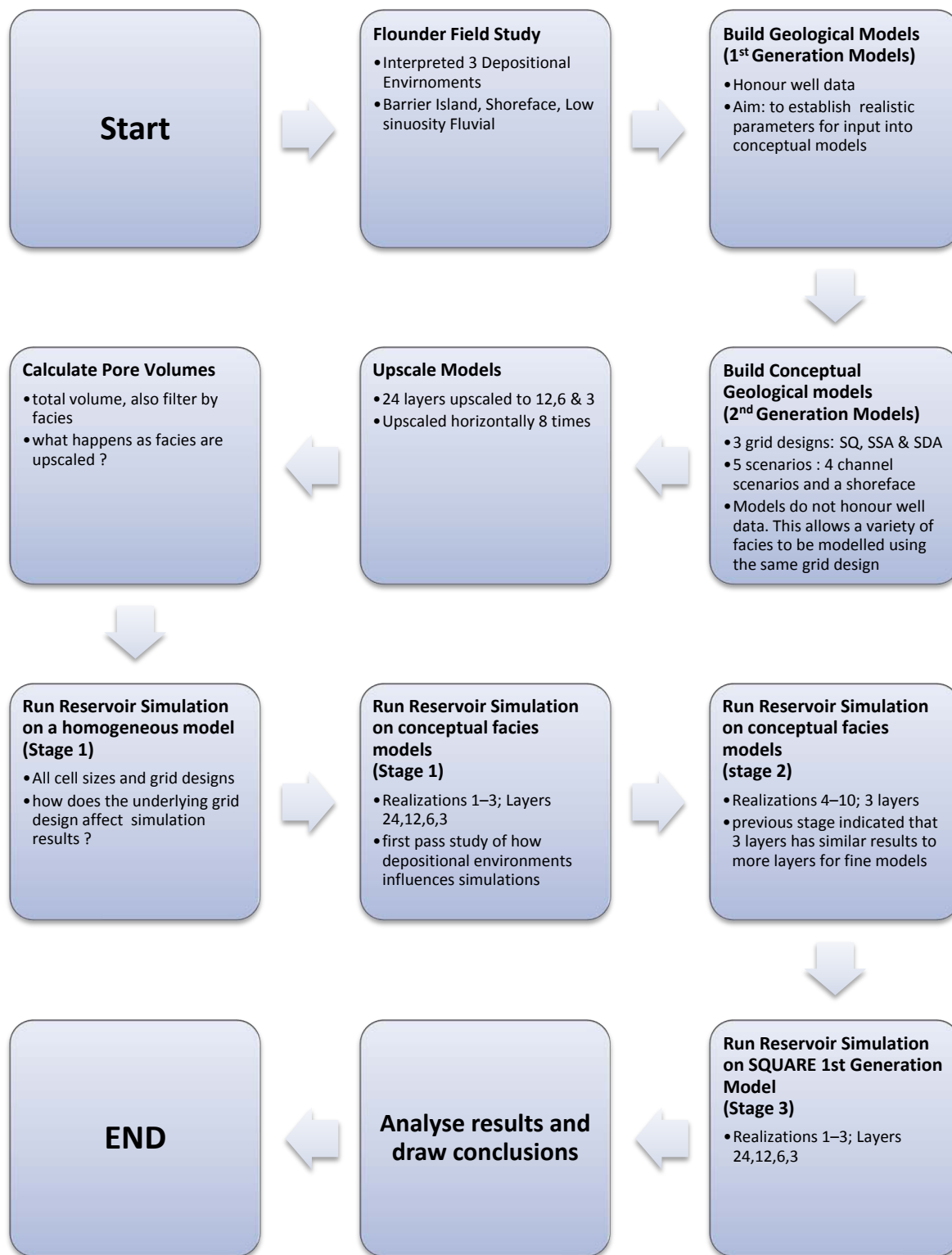
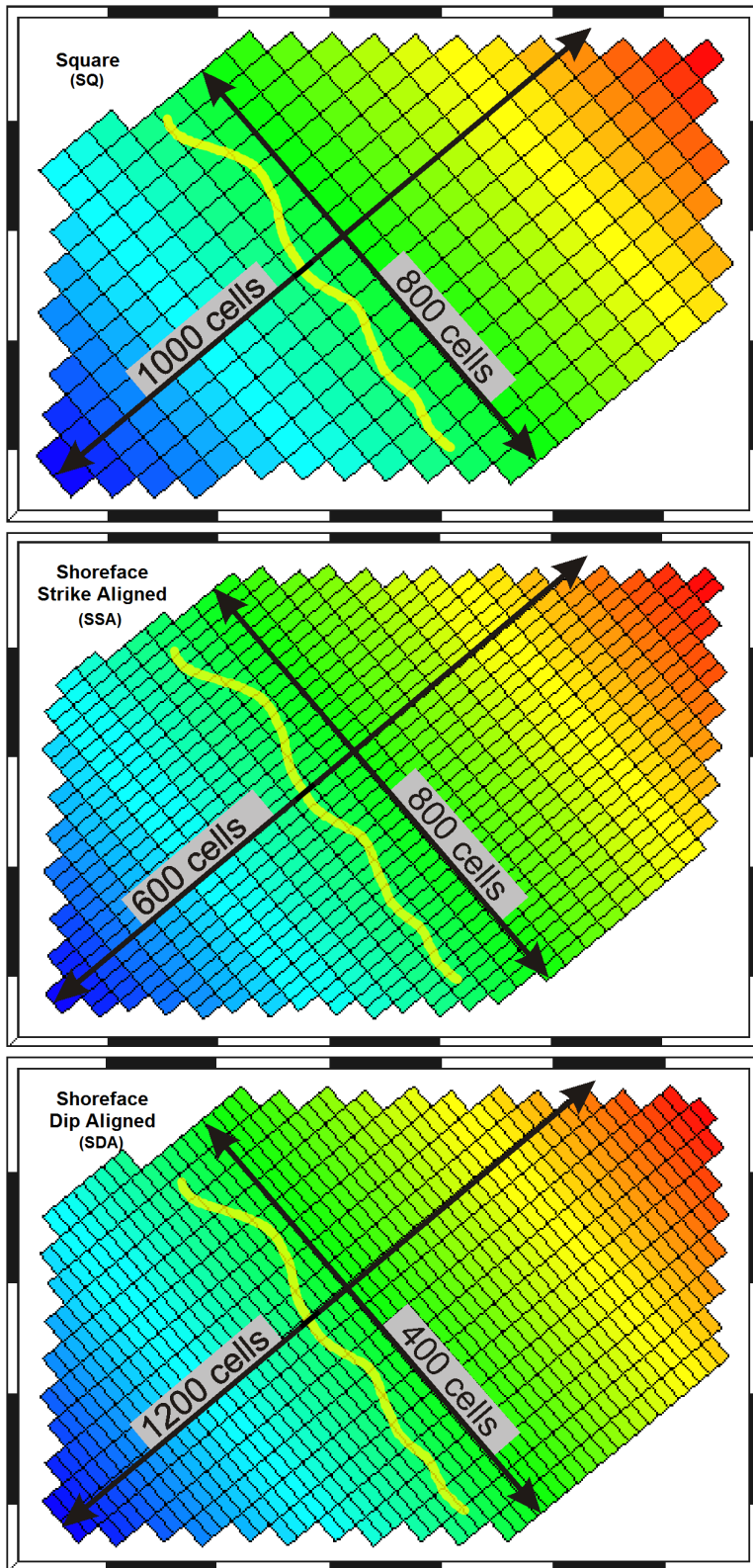
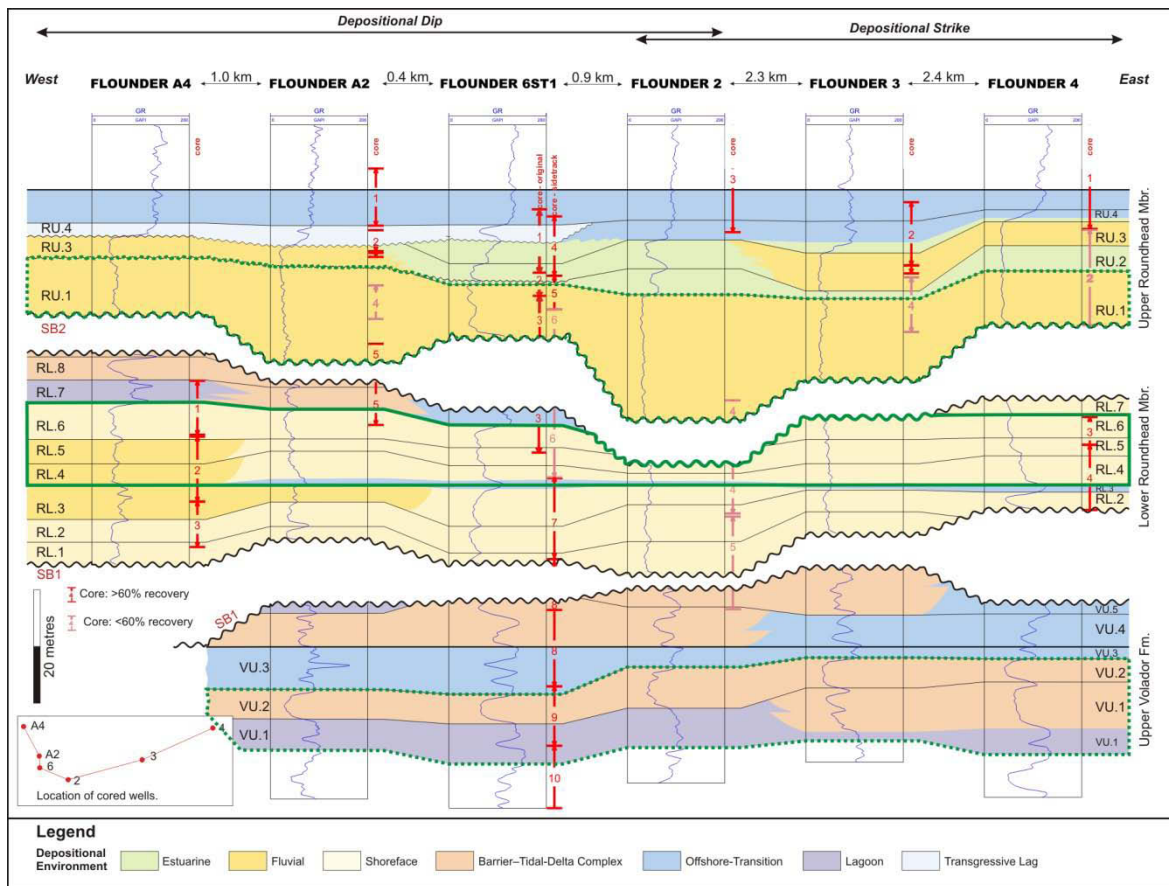


Figure 4.1. Brief flow path of modelling process for this study.



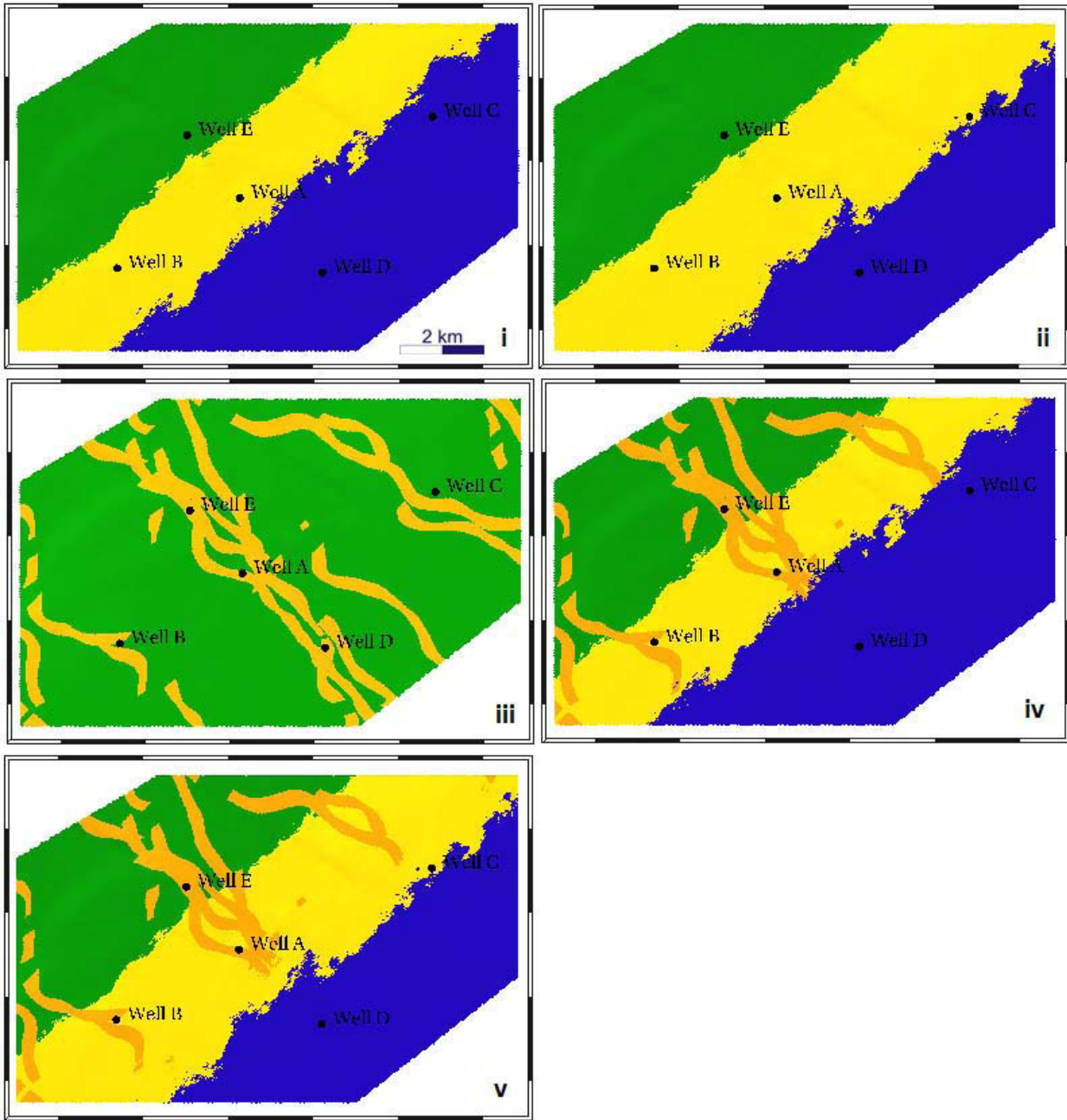
**Figure 4.2. RMS Screen captures showing the three grid designs used—Square, SSA and SDA.** All grids were rotated 40° to capture the main orientation of the coastline in the Flounder Field. The yellow lines indicate the orientation of the channels in the conceptual and Flounder models. The grids shown have been upscaled 40 times, thus clearly showing the arrangement of cells. The arrows (and text in grey boxes) indicate the number of cells in the base models.



**Figure 4.3. Cross section showing the upper Roundhead Member to upper Volador Formation interval.**

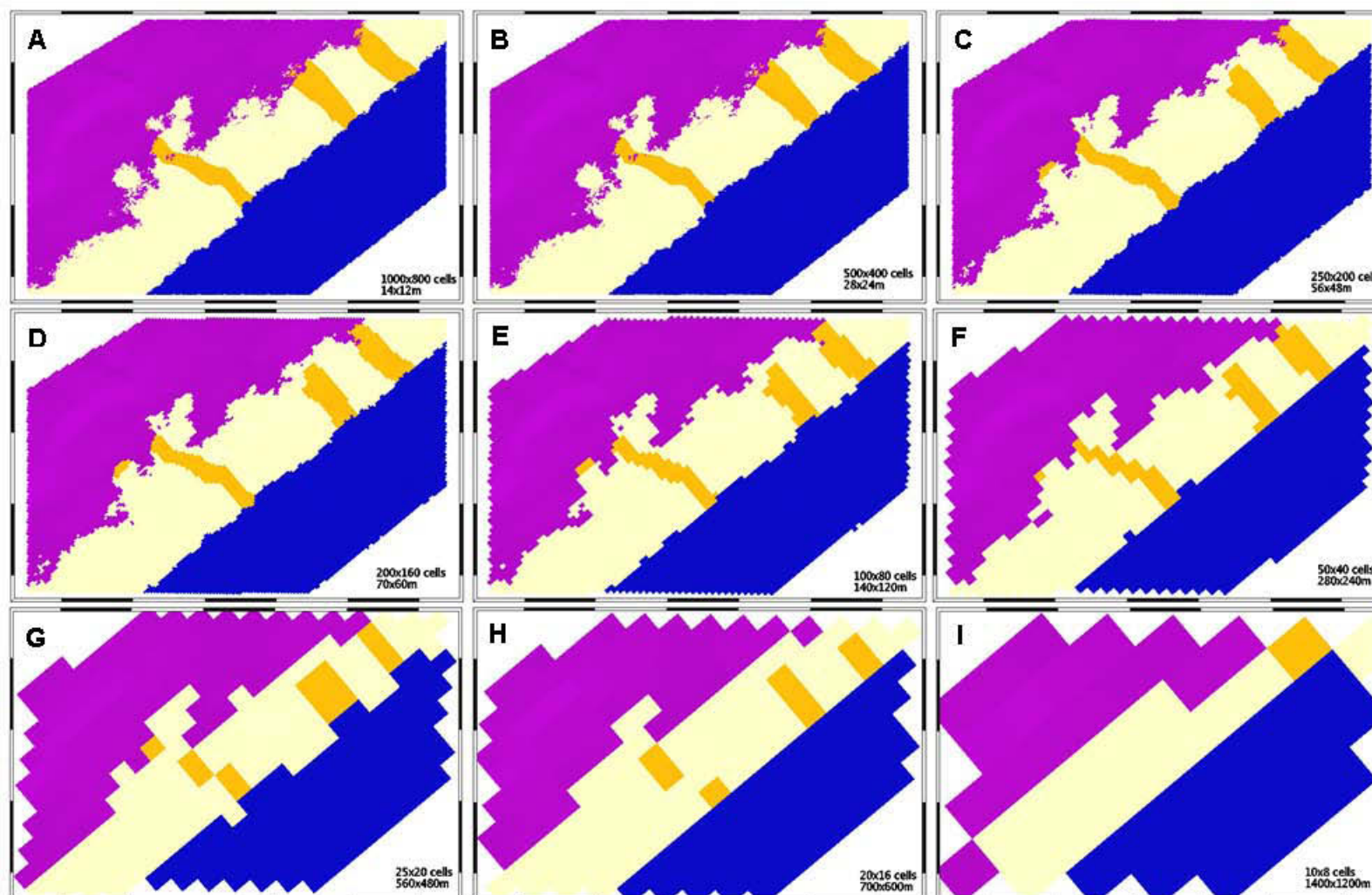
The interval used for the conceptual models (the top RL.6 to top RL.3 units) is surrounded by the solid green line. The top of the RL.6 unit; marks a shift from attached shoreface to barrier island system, whilst the top of the RL.3 unit is by a regional flooding surface. The dashed green lines show the intervals which were used for the models of the upper Volador Formation and the upper Roundhead Member models.

Each section is hung on a separate flooding surface. The datum for the upper Roundhead Member is a flooding surface above the RU.4 unit. The datum for the lower Roundhead Member is a flooding surface at the top of the RL.3 unit. This surface is the most widespread flooding surface within the lower Roundhead Member. The upper Volador Formation is datumed on the VU.3/VU.4 boundary. The VU.3 unit represents a brief marine transgression the covered the entire field with offshore transition sediments.

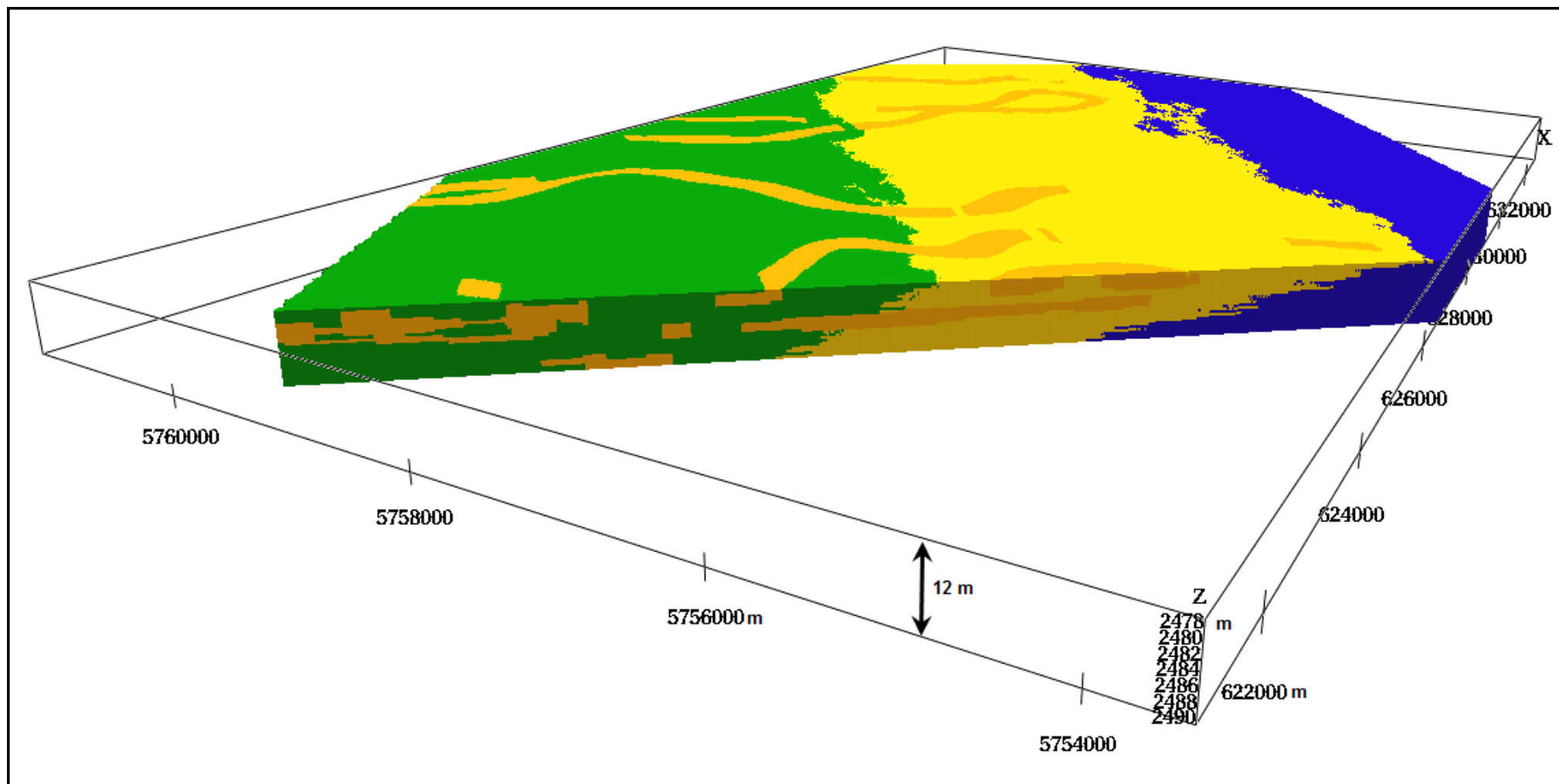


**Figure 4.4. Building the coastal facies model.** Step 1 is to build two prograding shoreface models using RMS’s ‘facies belt’ module—figures i and ii (Green=coastal plain, Yellow=shoreface, Blue=offshore marine). The shoreface in figure ii extends further seaward than that in figure i. Step 2 is to build a channel facies model (figure iii) using RMS’s ‘channels’ module. Channels are orange, overbank is green. Step 3 is to merge the first shoreface (Figure i) with the channel model (figure iii), to form a shoreface with fluvial influence (figure iv). This model (figure iv) is then merged with the second shoreface model (figure ii), to produce a transgressive shoreface model (figure v). The channel facies are interspersed with the shoreface sediment, but are reworked at interface with the offshore sediments.

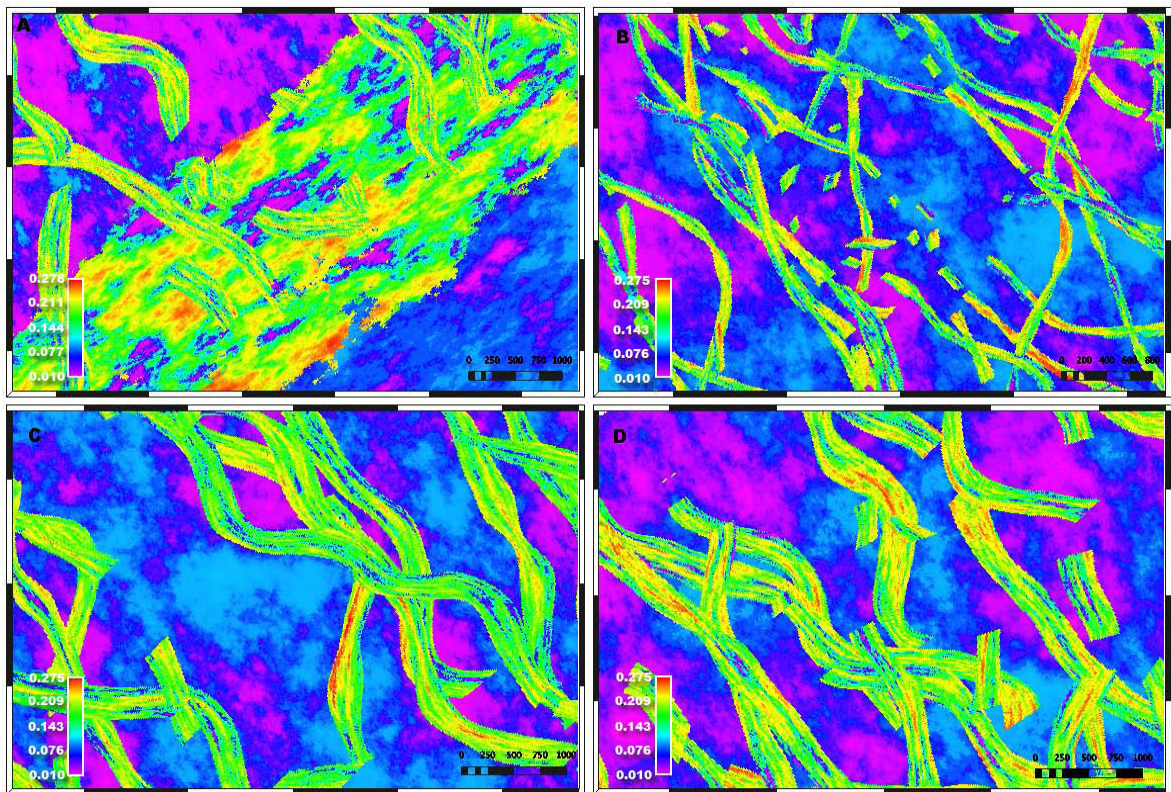




**Figure 4.5. Facies model of upper Volador Formation barrier island system.** Blue: offshore; pale yellow: barrier shoreface, washover fans and tidal deltas; orange: tidal channels and purple: lagoon. Once the model is upscaled beyond the half the width of the tidal channels (F), the morphology of the tidal channels changes significantly. Although the average width of the barrier is not distorted until the final upscale level (I), the detail of the washover fans and tidal delta complex is lost at a much smaller grid size.

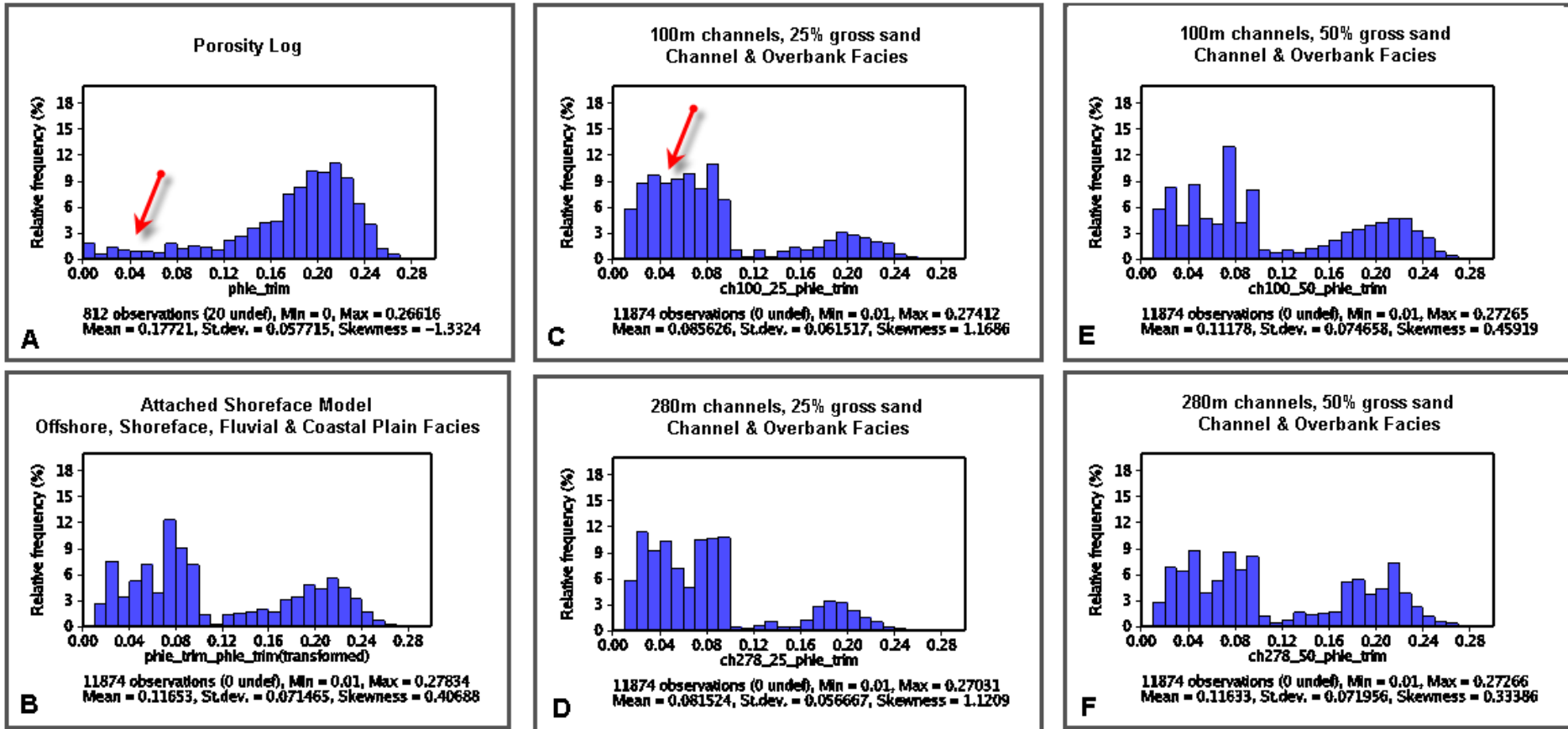


**Figure 4.6. Flattened section of shoreface facies model.** The angle of progradation of the offshore/shoreface boundary is lower than that of the shoreface/coastal plain interface. The different colours represent different facies: green = coastal plain, orange = fluvial channel, yellow = shoreface and blue = offshore marine. The shoreface progrades to the right of the model. There is significant vertical exaggeration.



**Figure 4.7. Porosity models—individual layers.** A: shoreface model, B: 100 m channels, 25% gross sand, C: 280 m channels, 25% gross sand, and D: 280 m channels, 50% gross sand.





**Figure 4.8. Porosity Distribution histograms.** Figure A is the distribution of the log data from the Flounder Field wells. The remaining figures are the distributions of porosity of the porosity models for Realization 1. The distributions of the porosity models are dominated by the low porosity values (red arrows) that are associated with the overbank facies. This facies is present in much smaller quantities in the actual well data than in the conceptual models, thus changing the porosity distribution compared to the well data. For the distribution of the ‘reservoir facies’ alone see Figure 4.9.

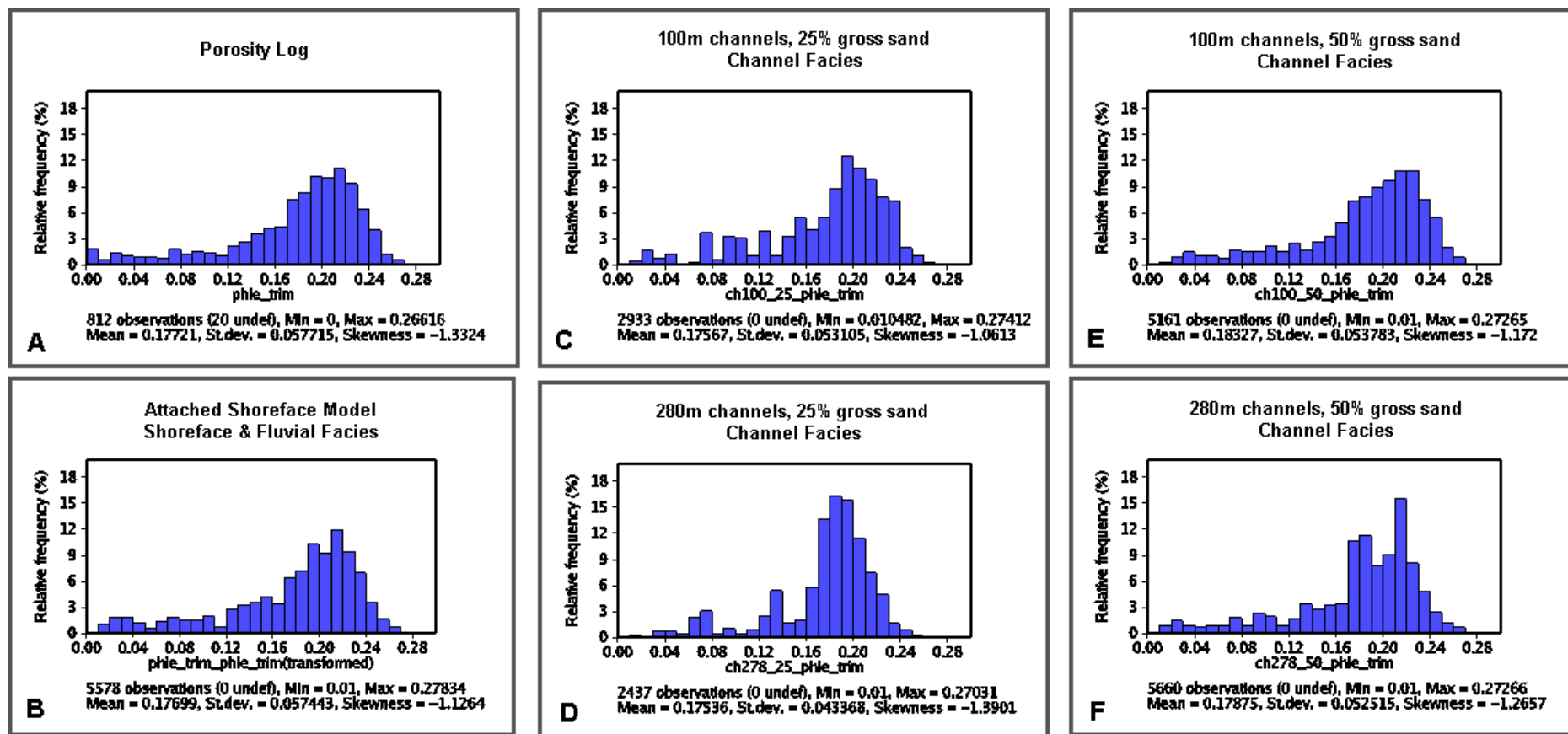
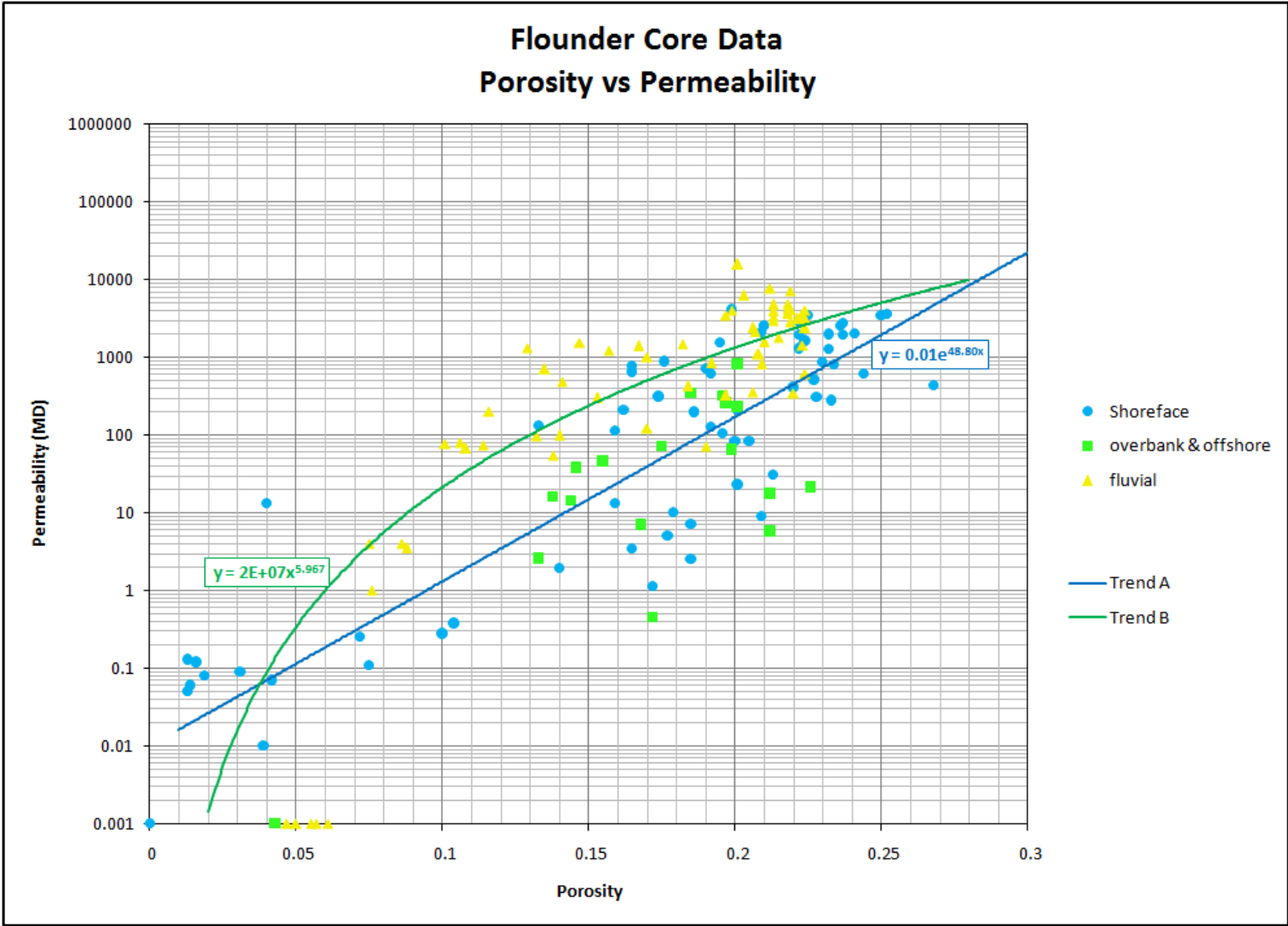


Figure 4.9. Porosity Distribution Histograms of reservoir facies. The reservoir facies in the conceptual models is very similar to that of the well data (of all facies).



**Figure 4.10. Cross plot of core porosity vs. core permeability.** Two trend lines have been used establish relationships between porosity and permeability for reservoir and non-reservoir facies. Trend A (blue) is the trend associated with the shoreface facies in the core. This trend is used for all reservoir facies in the model. Trend B is the relationship used for the offshore and coastal plain facies. This trend is derived from a mix of facies as the overbank and offshore data points alone would have produced higher than desired permeability values for low porosity values. Note: in the model, a high-end cut-off of 10% porosity is applied to the non-reservoir facies.